Botryoidal and Spherulitic Aragonite in Carbonates Associated with Microbial Mats: Precipitation or Diagenetic Replacement Product?

Yuzhu Ge[1]*, Giovanna Della Porta[2], Chelsea L. Pederson[1]*, Stephen W. Lokier[3], René Hoffmann[1] and Adrian Immenhauser[1,4]

[1]Institute for Geology, Mineralogy and Geophysics, Ruhr-Universität Bochum, Bochum, Germany, [2]Earth Sciences Department, University of Milan, Milan, Italy, [3]School of Ocean Sciences, Bangor University, Bangor, United Kingdom, [4]Fraunhofer IEG (Institution for Energy Infrastructures and Geothermal Systems), Bochum, Germany

Similar carbonate fabrics may result from different pathways of precipitation and diagenetic replacement. Distinguishing the underlying mechanisms leading to a given carbonate fabric is relevant, both in terms of an environmental and diagenetic interpretation. Prominent among carbonate fabrics are aragonite botryoids and spherulites, typically interpreted as direct seawater precipitates and used as proxies for fluid properties and depositional environments. This study investigated μm to mm-scale Holocene botryoidal and spherulitic aragonite from marine and non-marine carbonate settings associated with microbial mats, and reports two distinct formation mechanisms: 1) early diagenetic replacement, and 2) primary precipitation via nanocrystal aggregation. In the intertidal microbial mats of Khawr Qantur (Abu Dhabi), botryoidal and spherulitic aragonite are replacement products of heavily micritized bioclasts. To form the botryoidal and spherulitic aragonite, skeletal rods and needles, resulting from disintegration of micritized bioclasts, recrystallize into nanocrystals during early marine diagenesis. These nanocrystals then grow into fibrous crystals, forming botryoidal and spherulitic aragonite. In the lacustrine microbial bioherms of the hypersaline Great Salt Lake (United States) and in the hydrothermal travertines of Bagni San Filippo (Italy), botryoidal and spherulitic aragonite evolve from nanocrystals via precipitation. The nanocrystals are closely associated with extracellular polymeric substances in microbial biofilms and aggregate to form fibrous crystals of botryoidal and spherulitic aragonite. The studied fabrics form a portion of the bulk sediment and show differences in terms of their formation processes and petrological features compared to the often larger (few mm to over 1 m) botryoidal and spherulitic aragonite described from open-marine reefal cavities. Features shown here may represent modern analogues for ancient examples of carbonate depositional environments associated with microbialites. The implication of this research is that botryoidal and spherulitic aragonite associated with microbial mats are relevant in paleoenvironmental interpretations, but must be combined with a detailed evaluation of their formation process. Care must be taken as the term "botryoidal and spherulitic aragonite" may in fact include, from the viewpoint of their nucleation and formation mechanism, similar fabrics originated from different pathways. At present, it seems unclear to which degree

the µm to mm-scale botryoids and spherulites described here are comparable to their cm- to dm-size counterparts precipitated as cements in the open pore space of reefal environments. However, it is clear that the investigation of ancient botryoidal and spherulitic aragonite must consider the possibility of an early diagenetic replacement origin of these precipitates.

Keywords: botryoidal aragonite, spherulitic aragonite, precipitation, early replacement, microbial mats

INTRODUCTION

Early marine and non-marine carbonate precipitates are important environmental and diagenetic proxies used to study some of the most critical problems in carbonate research (Sandberg, 1983; Wilson and Dickson, 1996; Swart, 2015). Genetically different—but texturally similar—carbonate fabrics and early precipitates, however, can form in similar carbonate settings (Sandberg, 1985; Wilson and Dickson, 1996; Nielsen et al., 2005). For example, in microbial mats and during microbialite precipitation, the complex interaction between fluid physico-chemical properties, biofilm organic matter, microbial activity and carbonate minerals may result in similar carbonate fabrics that have, in fact, a different origin (Pope and Grotzinger, 2000; Jaramillo-Vogel et al., 2019). The differentiation between various mechanisms of carbonate crystal nucleation and precipitation is significant for geological interpretations. This study focuses on the diverse origin of botryoidal and spherulitic aragonite in three carbonate settings, each with specific fluid physico-chemical properties and depositional environments, but sharing the common presence of microbial mats. The aims of this study are to: 1) assess environmental conditions, processes, and mechanisms of the formation of botryoidal and spherulitic aragonite; and 2) provide guidelines for the interpretation of appropriate ancient analogues.

Botryoidal and spherulitic aragonite are spectacular fabrics found in Precambrian to Holocene marine (Ginsburg and James, 1976; Taviani and Rabbi, 1984; Aissaoui, 1985; Grotzinger and Kasting, 1993; Jaramillo-Vogel et al., 2019) and non-marine (Pentecost, 2005; Fouke, 2011; Capezzuoli et al., 2014; Della Porta, 2015 and references therein) carbonates. Hence, these carbonate growth-forms have been described from a wide range of depositional environments including: marine peritidal settings (Sumner and Grotzinger, 2000, 2004); reefs at carbonate platform margins and slopes (Ginsburg and James, 1976; Taviani and Rabbi, 1984; Aissaoui, 1985; Della Porta et al., 2003; van der Kooij et al., 2010; Jaramillo-Vogel et al., 2019); lacustrine environments (Della Porta, 2015; Pace et al., 2016), methane cold seeps (Peckmann et al., 1999; Feng et al., 2008; Himmler et al., 2010) and hydrothermal travertines (Folk, 1994; Pentecost, 2005; Fouke, 2011; Della Porta, 2015; Jones, 2017a, b). As both, botryoidal and spherulitic aragonite consist of aragonite fibers with a radial arrangement, they are often considered closely related fabrics (Ginsburg and James, 1976; Davies, 1977; Aissaoui, 1985). In marine settings, individual botryoids or similar fibrous crystal fan fabrics can range in size from a

few µm (Pleistocene; Taviani and Rabbi, 1984) to more than 1 m (Archean; Grotzinger and Kasting, 1993). Mostly reported from platform margin reefs, botryoidal and spherulitic aragonite generally nucleate on the walls of voids and grow in the direction of free pore space (Ginsburg and James, 1976; Davies, 1977; Taviani and Rabbi, 1984; Aissaoui, 1985). All of these fabrics have typically been interpreted as primary carbonate precipitates (Ginsburg and James, 1976; Handford et al., 1984; Aissaoui, 1985; van der Kooij et al., 2010; Jones, 2017a, Jones, 2017b). In contrast, a limited number of studies in (sub)recent and ancient carbonate settings (Shinn, 1969; Davies, 1977; Warren, 1982; Sandberg, 1985) proposed, albeit without providing details, a replacement origin for botryoidal and spherulitic aragonite.

With reference to marine reefal frameworks from Paleozoic, Mesozoic, or Cenozoic to Quaternary carbonate platforms, botryoidal aragonite precipitates often coexist with microbial carbonates (Mazzullo, 1980; Russo et al., 1997; Keim and Schlager, 2001; Della Porta et al., 2003; Riding, 2008; van der Kooij et al., 2010; Marangon et al., 2011; Jaramillo-Vogel et al., 2019). In hypersaline lacustrine settings fibrous spherulitic aragonite can form part of the precipitated framework of microbial bioherms (Della Porta, 2015; Pace et al., 2016; Vennin et al., 2019). In many carbonates older than Neogene in age, botryoidal and spherulitic fabrics are mineralogically preserved as calcite, dolomite, or chert (Sumner and Grotzinger, 2000), but under favorable conditions, their aragonite precursor mineralogy is recognizable by petrographic features and geochemical evidence (Davies, 1977; Mazzullo, 1980; Sumner and Grotzinger, 2000). The initial nucleation and precipitation processes of fossil botryoidal and spherulitic aragonite remain difficult to interpret, but can be inferred from modern analogues.

Given the significant biotic and environmental variations in Earth's history, (e.g. Sandberg, 1985), direct comparisons of processes and products must be made with the appropriate reservation. Along these lines, this study presents evidence that in reference to the studied µm to mm-scale botryoidal and spherulitic aragonite fabrics associated with microbial mats, similarities do exist and comparisons can be tentatively made with similar fabrics in the geological record, at least for those formed after the great oxidation event (Krumbein et al., 2003; Bekker et al., 2004; Anbar et al., 2007). Many studies of Phanerozoic botryoidal and spherulitic aragonite are biased toward wave-resistant reef frameworks, particularly those built by metazoan communities, (e.g. Ginsburg and James, 1976; Aissaoui, 1985). In contrast, Phanerozoic (particularly Cenozoic) botryoidal and spherulitic aragonite within

carbonate environments with microbial mats and microbial carbonate precipitation have received less attention in terms of origin and formation processes. Here we aim to better document μm to mm-scale Holocene botryoidal and spherulitic aragonite in various marine and non-marine carbonate depositional environments, where botryoidal and spherulitic aragonite fabrics are associated with microbial mats and microbialite formation. In contrast to the viewpoint of direct seawater precipitation, (e.g. Ginsburg and James, 1976), results documented here are in agreement with the more nuanced view indicating that (at least some) botryoidal and spherulitic aragonite may have multiple pathways of formation (Davies, 1977; Sandberg, 1985).

We document and discuss petrological features of botryoidal and spherulitic aragonites from three Holocene depositional environments with microbial mats and different water physico-chemical properties in order to enlighten the complex origins and formation processes of these fabrics associated with microbial mats. Results shown here are relevant as the recognition and interpretation of botryoidal and spherulitic aragonite in fossil records are important in both paleoceanography and general carbonate research, providing important information regarding water chemistry and depositional and diagenetic environments (Mazzullo, 1980; Aissaoui, 1985; Grotzinger and Kasting, 1993; Sumner and Grotzinger, 2000, Sumner and Grotzinger, 2004). We acknowledge that similar fabrics have also been reported from non-carbonate lithologies, (e.g. botryoidal calcite in ocean basalts; Lavoie, 1995) and we do not claim that the model presented here is universally applicable. We propose, however, that botryoidal and spherulitic aragonite associated with microbial mats are a prominent theme in carbonate research and one that is relevant over several billions of years of Earth's history.

TERMINOLOGY

Botryoidal (hemispheroidal) aragonite typically consists of individual or coalescing mamelons of fibrous crystals with squared-off terminations, and ranges in size from several μm to >1 m (Ginsburg and James, 1976; Grotzinger and Kasting, 1993). The term fibrous is used here to define crystals that are needle-like, elongated parallel to the c-axis with a length to width ratio >6:1 (cf. Flügel, 2010). In thin section, fibrous crystals forming the mamelons are generally μm to mm in size and tightly packed, with radial or fan-like structures causing sweeping extinction (Ginsburg and James, 1976; Aissaoui, 1985). Under the scanning electron microscope (SEM), euhedral and well-developed aragonite fibers with intimate interpenetration and blunt terminations are commonly observed (Ginsburg and James, 1976; Aissaoui, 1985). Where aragonitic mamelons have spheroidal arrangements, they are usually referred to as "spherulitic aragonite" (Davies, 1977; Aissaoui, 1985). In a broad sense, spherulite has been used to describe spherical bodies of various sizes, fabrics, and mineralogies (Verrecchia et al., 1995; Shtukenberg et al., 2012). Bates and Jackson (1980), p. 601, for example, described spherulites as "... more or less spherical body or coarsely crystalline aggregate with a radial internal structure arranged around one or more centers, varying

in size from microscopic grains to objects many centimeters in diameter, formed in a sedimentary rock in the place where it is now found…..." The terms "spherulites" and "spherulitic bodies" are further used in lacustrine (Mercedes-Martín et al., 2017), travertine (Folk, 1993; Jones, 2017a; Jones, 2017b), marine (Davies, 1977; Aissaoui, 1985), and vadose settings, (e.g. laminar calcretes with calcitic spherulites; Verrecchia et al., 1995). In the present study, the non-interpretative term "botryoidal aragonite" is employed to describe fans of fibrous crystals with non-spherical spatial organization and "spherulitic aragonite" is used to describe fibrous crystal structures with a spherical organization.
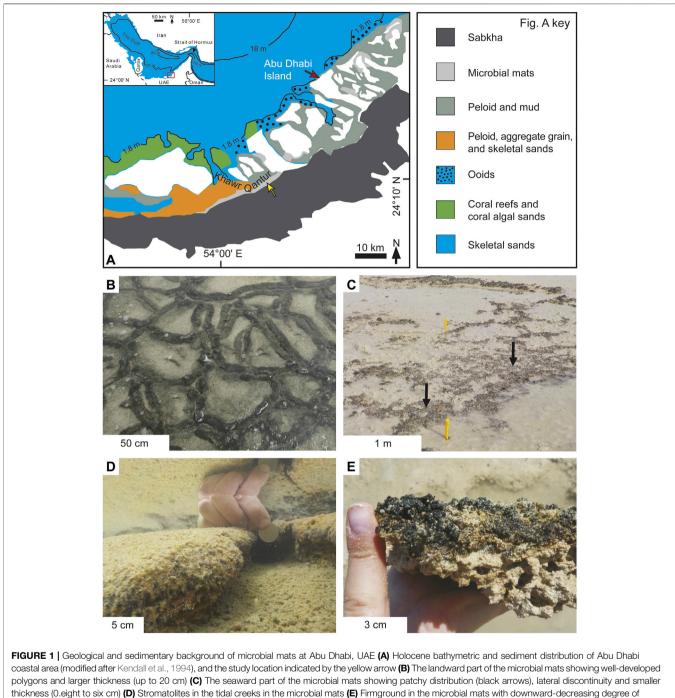
Carbonate mineral precipitation associated with microbial mats is the result of various and complex mineralization pathways resulting from the interaction between active microbial metabolic activity, passive organic matrices such as biofilm extracellular polymeric substances (EPS) and physico-chemical parameters, (e.g. alkalinity, pH, temperature, supersaturation with respect to $CaCO_3$) of the precipitating fluid (Riding, 2000; Dupraz et al., 2009 and references therein). In this study, the term "microbially mediated" is used with a broad meaning encompassing all processes of carbonate precipitation associated with microbial mats, including both biologically induced mineralization linked to microbial metabolism and biologically influenced mineralization related to passive mineralization of organic matter (Dupraz et al., 2009 and references therein).

In contrast to the original, comparably narrow definition of Folk (1959; micrite as a compound-acronym for "microcrystalline calcite"), the term micrite is here used in a somewhat wider sense and follows the revision as proposed by Folk (1974). Therefore, the term micrite is used to address fine-grained carbonate that is, for the most part, < 4 μm in size and appears translucent or dense in thin section, independent of the calcite or aragonite mineralogy (Bathurst, 1966; Folk, 1974; Reid et al., 1992). Hence, the micrite definition adopted in this study relies on crystal size limits including both calcite and aragonite micrite-grade carbonate (cf. Flügel, 2010). Clotted peloidal micrite describes in situ precipitated carbonate fabric made of clots of micrite- and microsparite-grade carbonate, often the product of microbially mediated carbonate precipitation (cf. Riding, 2000; Della Porta et al., 2003; Flügel, 2010; Della Porta, 2015 and references therein). Nanocrystal is used for crystals ≤1 μm in size sensu in Jones (2017b). Travertine represents terrestrial carbonate deposits produced from non-marine, supersaturated calcium bicarbonate-rich waters, typically hydrothermal in origin, as proposed by Pedley (1990), Ford and Pedley (1996), and Capezzuoli et al. (2014).

GEOLOGICAL AND SEDIMENTOLOGICAL BACKGROUND INFORMATION

Intertidal Microbial Mats, Abu Dhabi

The Abu Dhabi coastal area, located in the southern margin of the Persian Gulf (**Figure 1A**), represents a low-gradient (<0.1°) carbonate ramp on a modern subtropical epeiric sea

FIGURE 1 | Geological and sedimentary background of microbial mats at Abu Dhabi, UAE (A) Holocene bathymetric and sediment distribution of Abu Dhabi coastal area (modified after Kendall et al., 1994), and the study location indicated by the yellow arrow (B) The landward part of the microbial mats showing well-developed polygons and larger thickness (up to 20 cm) (C) The seaward part of the microbial mats showing patchy distribution (black arrows), lateral discontinuity and smaller thickness (0.eight to six cm) (D) Stromatolites in the tidal creeks in the microbial mats (E) Firmground in the microbial mats with downward-decreasing degree of cementation.

(Lokier and Fiorini, 2016). The climate is characterized by high temperature (>50°C in summer), low rainfall (average of 72 mm/yr) and strong seasonal winds (north-northwest Shamals) (Lokier and Fiorini, 2016; Ge et al., 2020a). Within a restricted intertidal environment at Khawr Qantur (**Figure 1A**), microbial mats are dominated by cyanobacteria, purple sulfur bacteria and sulfate-reducing bacteria (Scherf and Rullkötter, 2009). The mats can be

roughly divided into two zones: 1) a landward, well-developed, laterally continuous zone, with mats up to 20 cm thick characterized by the development of polygons >1 m wide (**Figure 1B**), and 2) a seaward zone where thinner (0.8–6 cm), poorly developed, discontinuous mats with patchy distribution (**Figure 1C**). Stromatolites (10–25 cm in relief; **Figure 1D**; Paul et al., 2020) are locally present in shallow tidal creeks (*ca* 20–40 cm water depth at low tide), which
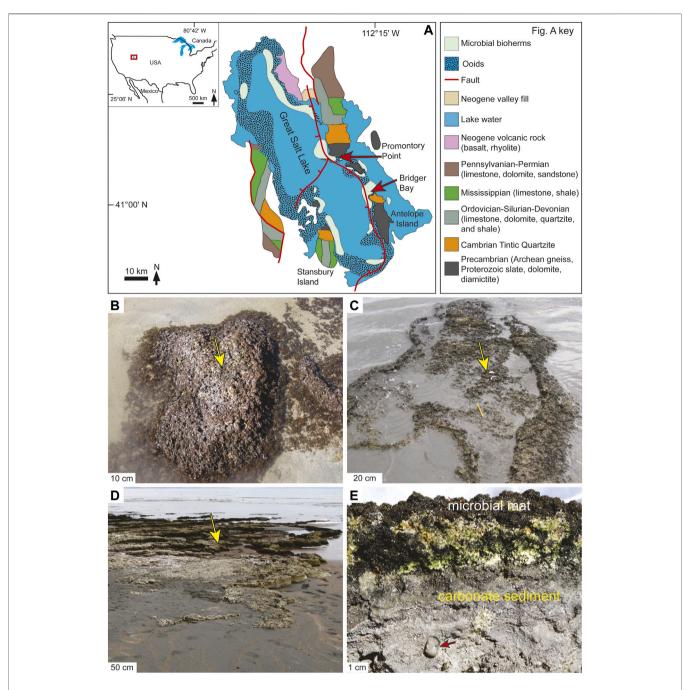
FIGURE 2 | Microbial bioherms in Great Salt Lake, Utah, United States (A) Schematic geological map of the Great Salt Lake (modified after Della Porta, 2015 and references therein) showing faults extracted from Colman et al. (2002) and distribution of microbial bioherms and ooidal sand from Eardley (1938) and Carozzi (1962). Sampling locations of Promontory Point and Bridger Bay marked by red arrows (B) Isolated roughly circular microbial bioherms (arrowed) at Bridger Bay (C) Elongated microbial bioherms (arrowed) at Promontory Point (D) The belt formed by adjacent microbial bioherms (arrowed) surrounded by ooidal peloidal sand at Promontory Point (E) Architecture of the microbial bioherm showing an upper layer consisting of microbial mats and a lower part consisting of precipitated carbonate sediment. Note a gastropod (red arrow) in the carbonate sediment.

locally undercut the microbial mats and shallow landwards. Beneath the mats, firmgrounds (**Figure 1E**) containing botryoidal and spherulitic aragonite are laterally separated by unconsolidated bioclastic and peloidal carbonate sediments. The firmgrounds shallow in a seaward direction, from *ca* 15 cm beneath the microbial mats surface to exposure

at the sediment-water interface over a distance of *ca* 330 m, with a corresponding decrease in thickness (from 20 to 0.2 cm) and lateral continuity of the overlying mats. The landward firmgrounds are light gray in color and have an H_2S odor, whereas the seaward firmgrounds are gray-to-beige in color without any obvious H_2S odor. Dominating carbonate

mineralogies are aragonite and high-Mg calcite (Paul and Lokier, 2017; Ge et al., 2020a).

Littoral Microbial Bioherms, Great Salt Lake

As a remnant of the Pleistocene Lake Bonneville, the Great Salt Lake (Utah, United States; **Figure 2A**) is an endorheic polymictic hypersaline lake (Eardley, 1938) controlled by faults (Colman et al., 2002). The climate is semi-arid with moderate rainfall (average of 125–375 mm/yr) and a temperature range of −8–26°C (Kowalewska and Cohen, 1998; Wen, 2015). Rainfall is seasonal, concentrated in spring and fall with a dry season from June to July (Eardley, 1938; Kowalewska and Cohen, 1998). The lake margin is a low-angle, high-energy ramp, characterized by aragonitic ooidal sands and microbial bioherms (Eardley, 1938; Sandberg, 1975; Pedone and Folk, 1996; Reitner et al., 1997; Chidsey et al., 2015; Della Porta, 2015; Bouton et al., 2016; Pace et al., 2016; Lindsay et al., 2017; Baxter, 2018; Vanden Berg, 2019; Vennin et al., 2019). Great Salt Lake microbial communities include halophilic archaea, heterotrophic bacteria with most abundant *Marinimicrobium haloxylanilyticum* (Gram negative gammaproteobacteria polysaccharide-degrading heterotroph), sulfate-reducing bacteria, cyanobacteria and diatoms (Reitner et al., 1997; Kjeldsen et al., 2007; Pace et al., 2016; Baxter, 2018; Lindsay et al., 2017, Lindsay et al., 2020).

In the north-eastern area of Bridger Bay (NW of Antelope Island), microbial bioherms form roughly circular domes (**Figure 2B**). The relief of these domes ranges from 10 cm (on average) for those temporarily exposed along the shoreline, to nearly 1 m for those at 1–4 m depth (Della Porta, 2015). The bioherms can occur as isolated circular structures with a diameter of 0.2–1.2 m, or coalesce into clusters reaching up to 9 m in diameter. At Promontory Point (**Figure 2A**), microbial bioherms are lenticular and elongated in shape (**Figure 2C**), with widths of 0.2–4 m and lengths from 1 to 10 s of meters. These elongated bioherms are closely adjacent to each other, forming a discontinuous, *ca* 6 km wide belt subparallel to the shoreline over a distance of a few 10 s of meters to 2–3 km perpendicular to the shoreline (**Figure 2D**; Della Porta, 2015). Despite different morphologies, all microbial bioherms show similar internal architecture, with an outer mm to cm-thick microbial mat (**Figure 2E**), and an inner framework of precipitated carbonates, consisting of clotted peloidal micrite, laminated micrite and botryoidal and spherulitic aragonite (cf. Della Porta, 2015). The carbonates are mineralogically dominated by aragonite, but include also calcite and dolomite (Della Porta, 2015; Pace et al., 2016; Dunham et al., 2020).

Hydrothermal Travertines, Bagni San Filippo

Central Italy has been a site of widespread hydrothermal travertine deposition since the Neogene, (e.g. Chafetz and Folk, 1984; Guo and Riding, 1992; Faccenna et al., 2008; Capezzuoli et al., 2014; Della Porta, 2015; Croci et al., 2016; Della Porta et al., 2017a, b). The formation of travertine deposits is related to volcanic activity and extensional and strike-slip faults linked to the opening of the Tyrrhenian Sea as a back-arc basin
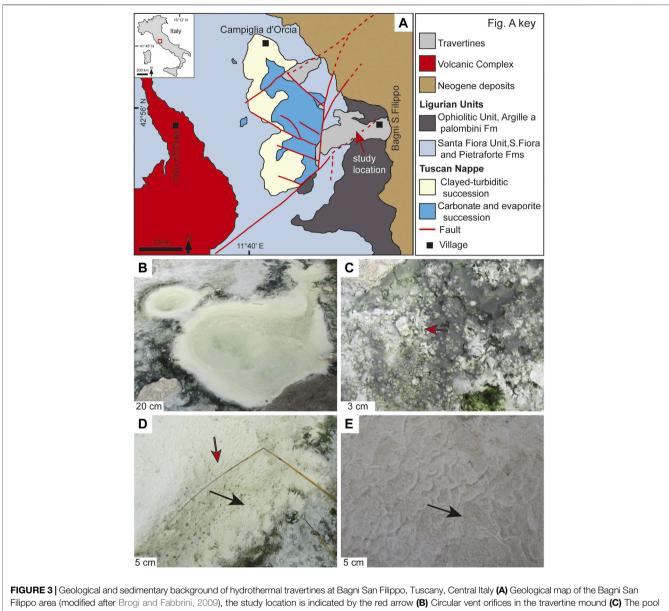
from the Late Miocene (Malinverno and Ryan, 1986; Doglioni, 1991; Patacca et al., 1992; Minissale, 2004; Carminati and Doglioni, 2012). In Bagni San Filippo (**Figure 3A**), extensive Pleistocene and present-day hydrothermal fluid circulation and travertines develop within the Mountain Amiata volcano geothermal area (Brogi and Fabbrini, 2009). Present-day travertine deposits in Bagni San Filippo precipitate from thermal water with a temperature of 47–52°C and pH of 6.5–6.7 in active vents (Pentecost, 1995; Minissale, 2004). The travertines are dominantly calcitic; however, close to the vent aragonite may locally precipitate at water temperatures >40°C (cf. Folk, 1994; Pentecost, 1995). Several studies have shown that travertine hydrothermal settings host diverse microbial mats as a function of water temperature and chemistry, including thermophilic archaea, sulfide-oxidizing bacteria, purple and green sulfur bacteria, filamentous green non-sulfur anoxygenic photoautotroph Chloroflexi, sulfate-reducing bacteria and cyanobacteria (Folk, 1993; Allen et al., 2000; Farmer, 2000; Pentecost, 2003, Pentecost, 2005; Fouke, 2011; Della Porta et al., 2021).

Actively forming travertine deposits comprise a *ca* 10 m thick mound with a central vent and steeply dipping slopes at Bagni San Filippo (Della Porta et al., 2021). The central vent consists of a horizontal pool (1.five to two m wide) with three 20–40 cm wide circular vent orifices (**Figure 3B**). Hydrothermal fluids emerge from the vent orifices and flow along a channel (30–40 cm wide) following the topographic gradient. The pool surrounding the vent orifices contains 1–2 cm deep stagnant water with thin (*ca* 0.1–1 mm) rafts and coated gas bubbles (**Figure 3C**). The travertine fabrics at the vent orifices consist of crystalline crusts and carbonate encrusted filamentous streamers (**Figure 3D**) of microbial mats (labeled as bacterial streamers by Farmer, 2000 in Yellowstone travertine deposits). In the channel departing from the vent, the travertine fabrics experience a series of changes at increasing distance from the vent. Crystalline crusts and encrusted filamentous streamers (**Figure 3D**) dominate in the initial 5 m and laterally shift into crystalline crusts with coated gas bubbles. Subsequently, the crystalline crusts with coated gas bubbles change into a micro-terraced (mm to cm-scale) system (**Figure 3E**), which forms cm-wide pools containing clotted peloidal micrite dendrites, coated grains, and coated gas bubbles. Sparse botryoidal and spherulitic aragonite only occur in the travertines precipitated along the first 5 m adjacent to the vent where temperature is > 44°C (Della Porta et al., 2021).

FIELDWORK AND METHODOLOGY

Fieldwork

At Khawr Qantur (N 24°9.780′, E 54°7.908′; **Figure 1A**), Abu Dhabi, carbonate firmgrounds were sampled along a landward-seaward transect in the intertidal microbial mat zone. In the Great Salt Lake, United States, samples were collected from microbial bioherms along the eastern lake shorelines at Bridger Bay (N 41°3.354′, W 112°15.148′) and Promontory Point (N 41°12.201′, W 112°26.499′) (**Figure 2A**). In Bagni San Filippo (N 42°55.633′,

FIGURE 3 | Geological and sedimentary background of hydrothermal travertines at Bagni San Filippo, Tuscany, Central Italy **(A)** Geological map of the Bagni San Filippo area (modified after Brogi and Fabbrini, 2009), the study location is indicated by the red arrow **(B)** Circular vent orifices in the travertine mound **(C)** The pool surrounding the vent orifices with 0.1–1 mm thick rafts and coated gas bubble (red arrow) on the stagnant water **(D)** Encrusted filamentous streamers (red arrow) near the vent; black arrow indicates thermal water flow direction **(E)** Micro-terraced (mm to cm-scale) travertines along a channel nearly 20 m away from the vent; black arrow indicates slope dip and thermal water flow direction.

E 11°41.692′; **Figure 3A**), Italy, travertine samples were collected at the hydrothermal vent where the temperature ranges from 44 to 49°C.
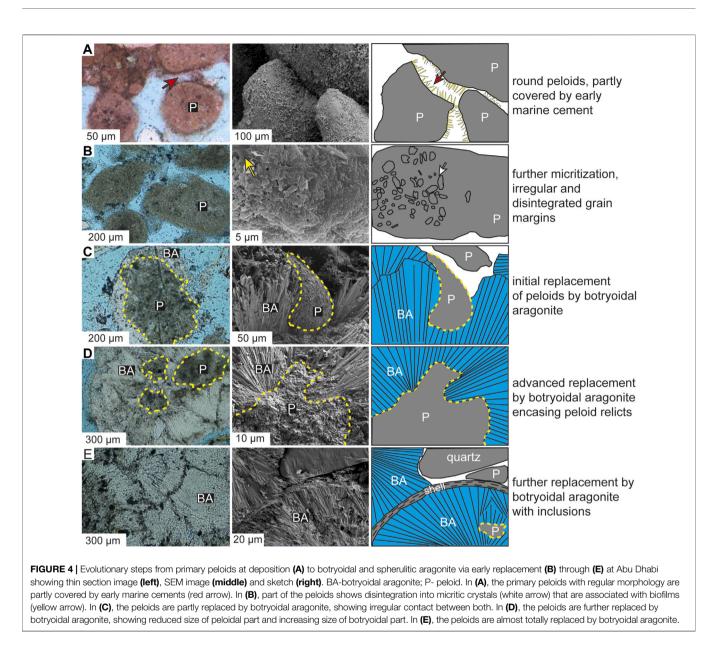
Optical Analyses

Samples were petrographically investigated by means of optical microscopy (Zeiss) and scanning electron microscopy (FESEM, Merlin Gemini II by ZEISS and Nordlys detector by OXFORD Instruments). For SEM analysis, the samples were cut into smaller pieces, cleaned with deionized water, and sputter coated with gold for imaging. The Abu Dhabi samples were analyzed at Ruhr-Universität

Bochum, Germany (ZEISS-Gemini 2-Merlin HR-FESEM), while the samples from Great Salt Lake and Bagni San Filippo were analyzed at University of Milan, Italy (Cambridge Stereoscan 360). The SEM operated at acceleration voltage of 2–20 kV, and working distances of 3–22 mm.

Water Chemistry

Where possible, water temperature and pH were measured in the field. A handheld Ultrameter™ Model 6P (Myron L Company, United States) was used in Abu Dhabi, and a handheld SevenGo Duo pro™ pH/ORP/Ion/Conductivity meter SG78 (Mettler

FIGURE 4 | Evolutionary steps from primary peloids at deposition **(A)** to botryoidal and spherulitic aragonite via early replacement **(B)** through **(E)** at Abu Dhabi showing thin section image **(left)**, SEM image **(middle)** and sketch **(right)**. BA-botryoidal aragonite; P- peloid. In **(A)**, the primary peloids with regular morphology are partly covered by early marine cements (red arrow). In **(B)**, part of the peloids shows disintegration into micritic crystals (white arrow) that are associated with biofilms (yellow arrow). In **(C)**, the peloids are partly replaced by botryoidal aragonite, showing irregular contact between both. In **(D)**, the peloids are further replaced by botryoidal aragonite, showing reduced size of peloidal part and increasing size of botryoidal part. In **(E)**, the peloids are almost totally replaced by botryoidal aragonite.

Toledo, Germany) was used at the Great Salt Lake and Bagni San Filippo. At Abu Dhabi, salinity, alkalinity and elemental concentrations of seawater were also measured following the protocol defined in Ge et al. (2020a).

Mineralogy and Crystallography

Mineralogy of Abu Dhabi samples was determined at Ruhr-Universität Bochum by energy dispersive spectroscopy (EDS) and electron backscatter diffraction (EBSD) analyses to produce mineralogy maps. The EBSD map processing included a step width of 1.54 µm, a beam energy of 20 kV, a working distance of 26 mm, and a tilt angle of 70°. These maps also produced the crystallographic orientation data. Mineralogy of Great Salt Lake and Bagni San Filippo carbonate samples was determined by EDS and an X-ray

Powder Diffractometer Philips X'Pert MPD with a high temperature chamber at University of Milan.

Carbon (δ^{13}C) and Oxygen (δ^{18}O) Isotope Geochemistry

Bulk samples of the Abu Dhabi firmgrounds were analyzed for $\delta^{13}C_{carb}$ and $\delta^{18}O_{carb}$, whereas the samples from the Great Salt Lake and Bagni San Filippo were micro-drilled to separate different micrite fabrics. All samples were analyzed at Ruhr-Universität Bochum, where 100–120 µg of sample powder was reacted with 85% H_3PO_4 at room temperature to produce CO_2. The CO_2 was analyzed using a FINNIGAN MAT Delta S Mass Spectrometer. NBS (National Bureau of Standards) standards were used to express the isotope results in V-PDB

TABLE 1 | Sediment and water properties (temperature, salinity, TDS, pH, alkalinity, Ca, Mg, Sr, Mg/Ca and aragonite saturation) of the three study areas.

	Microbial mats	Microbial bioherms	Hydrothermal travertines
Location	Khawr Qantur, Abu Dhabi, UAE	Great Salt Lake, Utah, United States	Bagni San Filippo, Italy
Climate	Subtropical, hot, arid	Continental, semi-arid	Mediterranean, temperate
Environment	Intertidal lagoon, marine	Endorheic, hypersaline lake	Hydrothermal spring and channel
Dominant sediment composition	Microbialite, aggregate grains, peloids, bioclasts, gypsum	Microbialites, oncoids, aggregate grains, peloids, ooids, gypsum, halite	Encrusted filamentous microbes forming streamers, micro-terraced crystalline dendrites, coated grains, coated reeds, gypsum
Mineralogy of botryoidal and spherulitic fabrics	Aragonite	Aragonite	Aragonite
Botryoidal and spherulitic fabrics	Aragonite botryoid and spherulite (20–300 μm in diameter) embedded in peloidal components, more spherulites in a landward direction	Aragonite spherulite (5–30 μm in diameter) embedded in clotted peloidal micrite	Aragonite spherulite (10–300 μm in diameter) embedded in dominantly calcitic travertines made of clotted peloidal micrite, rare botryoidal fans close to vents
Water temperature (°C)	21–31	2.2–25.3[e]	44–52[a,b]
Salinity (ppt)	50–107		
TDS (ppt)	83–220	138–276[c]	4.128[a]
pH	7.14–8.48	7.6–8.8[d]	6.5–6.7[a,b]
Alkalinity (mmol/l)	1.8–3.2	5.4–8.4[d]	27.8–30.1[a,b]
Ca (ppm)	478.99–697.23	150–510[e]	721–798[a,b]
Mg (ppm)	1,468–2,679	1700–16200[e]	182–198[a,b]
Sr (ppm)	9.03–13.15	2.1[f]	13.2[a]
Mg/Ca (mole ratio)	4.84–6.53	9.6–115.7[g]	0.59–1.19[h]
Aragonite saturation (Ω_{arg})	12–17	4–10[i]	10[b]

Included data sources:
[a]*Minissale (2004)*
[b]*Pentecost (1995)*
[c]*Eardley (1938)*
[d]*Reitner et al. (1997)*
[e]*Kowalewska and Cohen (1998)*
[f]*Livingstone (1963)*
[g]*Pedone and Folk (1996)*
[h]*Duchi et al. (1978)*
[i]*Dunham et al. (2020); those without indication are from this study.*

(Vienna-Pee Dee Formation belemnite) notation. The analytical precision was better than 0.07‰ for $\delta^{13}C$ and 0.13‰ for $\delta^{18}O$.
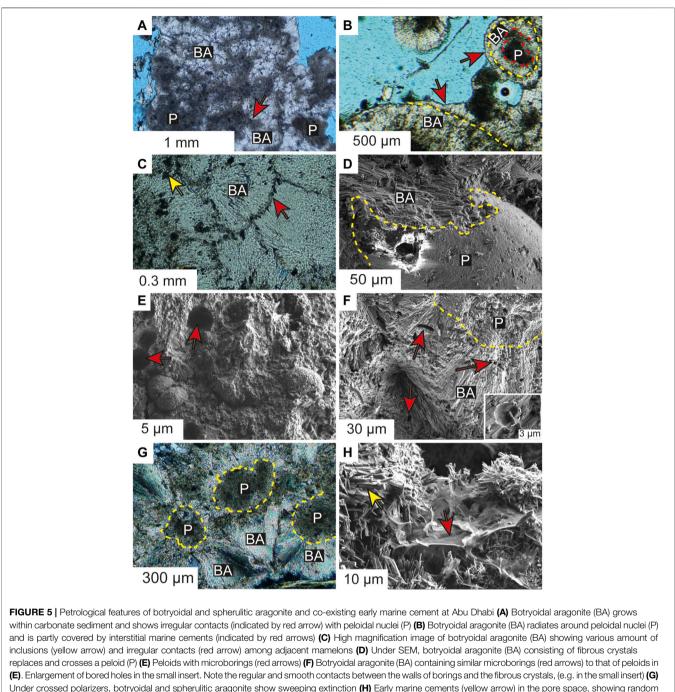
BOTRYOIDAL AND SPHERULITIC ARAGONITE IN CARBONATE SETTINGS ASSOCIATED WITH MICROBIAL MATS

Botryoidal and Spherulitic Aragonite From the Microbial Mats of Abu Dhabi

Associated with the intertidal microbial mats, the grains within firmgrounds mainly consist of extensively micritized peloids (**Figure 4A**), and minor amounts of bioclasts including gastropods, foraminifera, ostracods, and bivalves. Aggregate grains, quartz, and gypsum are also present (**Table 1**). With an increasing degree of micritization, the morphologies of the peloids evolve from regularly rounded to irregularly corroded with diffuse margins formed by μm size crystals (**Figure 4B**). Under SEM, the outer portions of peloids, including the diffuse margins, show fragmented, randomly arranged skeletal (components derived from skeletons) rods and needles (up to 10 μm length and <1 μm width) (**Figure 4B**), often bound by biofilms and associated with microborings. Morphologically

similar skeletal rods and needles comprise basic building units of some bioclast ultrastructures.

In the firmgrounds, aragonitic (**Table 1**) botryoidal and spherulitic fabrics are common and randomly oriented (**Figures 4C–E** and **Figure 5**; **Supplementary Figure S1**). These fabrics typically consist of coalescing mamelons (40–250 μm long) often (but not always) radially arranged around micritic peloidal nuclei, morphologically similar to irregular and corroded peloids (**Figures 4C,D** and **Figures 5A,B**). The botryoidal and spherulitic aragonite show gradual and irregular contacts with their associated nuclei (**Figure 5A**) and are partially coated by interstitial aragonite cements (**Figure 5B**). The botryoidal and spherulitic aragonite also contain micrite inclusions (**Figure 5C**) and have serrated contacts between adjoining mamelons (**Figure 5C**). The growth-front of botryoidal aragonite cross-cuts peloid interiors (**Figure 5D**). Botryoidal and spherulitic aragonite display sweeping extinction (**Figure 5G**) under crossed-polarized light. Under SEM, the botryoidal and spherulitic aragonite consist of radially oriented euhedral fibrous crystals (20–300 μm long and 0.13–1 μm wide) with flattened terminations (**Figure 4D** and **Figure 5F**). The crystals are densely packed (**Figure 5F**) and often associated with biofilms, while the micritic nuclei consist of relict peloids (**Figure 5D**) or aggregations of spheroidal nanocrystals

FIGURE 5 | Petrological features of botryoidal and spherulitic aragonite and co-existing early marine cement at Abu Dhabi **(A)** Botryoidal aragonite (BA) grows within carbonate sediment and shows irregular contacts (indicated by red arrow) with peloidal nuclei (P) **(B)** Botryoidal aragonite (BA) radiates around peloidal nuclei (P) and is partly covered by interstitial marine cements (indicated by red arrows) **(C)** High magnification image of botryoidal aragonite (BA) showing various amount of inclusions (yellow arrow) and irregular contacts (red arrow) among adjacent mamelons **(D)** Under SEM, botryoidal aragonite (BA) consisting of fibrous crystals replaces and crosses a peloid (P) **(E)** Peloids with microborings (red arrows) **(F)** Botryoidal aragonite (BA) containing similar microborings (red arrows) to that of peloids in **(E)**. Enlargement of bored holes in the small insert. Note the regular and smooth contacts between the walls of borings and the fibrous crystals, (e.g. in the small insert) **(G)** Under crossed polarizers, botryoidal and spherulitic aragonite show sweeping extinction **(H)** Early marine cements (yellow arrow) in the pore space, showing random distribution and association with biofilm EPS (red arrow).

(crystals ≤1 μm in size, and generally 100–700 nm in diameter). There are morphologically and dimensionally similar microborings (2–10 μm in diameter) in both the nuclei and surrounding fibrous crystals (**Figures 5E,F**). The microborings show smooth and regular contacts with the fibrous crystals. The botryoidal and spherulitic aragonite mainly grow toward the interiors of the micritic nuclei rather than into the interstitial pore space. In comparison, early marine aragonitic cements occupying open pore space show competitive growth toward free pore space, smaller sizes (2–15 μm long), various morphologies (platy to acicular) and flattened to pointed terminations (**Figure 5H**).

Corresponding chemical properties of seawater above the described firmgrounds containing botryoidal and spherulitic aragonite include high salinity and high aragonite saturation, as shown in **Table 1**. Isotope values of bulk firmground samples
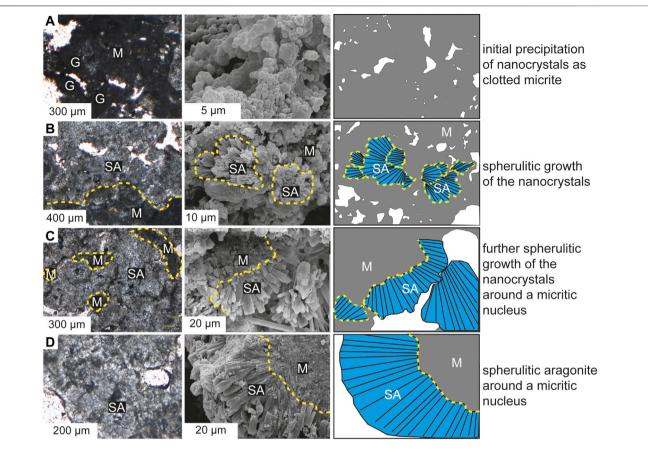
FIGURE 6 | Evolutionary steps from nanocrystals forming part of clotted peloidal micrite to botryoidal and spherulitic aragonite via precipitation and aggregation in Great Salt Lake microbial bioherms showing thin section image **(left)**, SEM image **(middle)** and sketch **(right)**. M-micrite, SA-spherulitic aragonite. In **(A)**, the clotted micrite consists of numerous nanocrystals with a random distribution. In **(B)**, aragonite fibers of spherulitic aragonite grow out from nanocrystals of micrites, and irregular contacts are between both. In **(C)**, aragonite fibers continue to grow on the micrite nucleus. In **(D)**, spherulitic aragonite increases in size and associated micrite decreases in abundance.

are lower in a landward direction ($\delta^{13}C_{carb} = 0‰$, $\delta^{18}O_{carb} = 0‰$) relative to the more seaward location ($\delta^{13}C_{carb} = 3.9‰$; $\delta^{18}O_{carb} = 2.9‰$).

Botryoidal and Spherulitic Aragonite in the Microbial Bioherms of Great Salt Lake

The lake-margin microbial bioherms display superficial 1–5 mm to 1 cm thick brown-orange to dark green microbial mats overlying the precipitated carbonates (**Figures 2B–E**). The microbial mats show limited signs of calcification whereas just below the microbial mat carbonate precipitates display a dark gray color (**Figure 2E**). Petrographic analysis shows that the precipitated carbonates are mainly composed of clotted peloidal micrite, i.e., microcrystalline carbonate forming clots with irregular to peloidal outlines (**Figure 6A**), irregular threads of fibrous crystals arranged in spherulites (**Figures 6B–D**), and other components including oncoids, aggregate grains, peloids and fecal pellets, ooids, pyrite, and rare halite and gypsum (**Table 1**). Fecal pellets are possibly produced by brine shrimp, and are embedded within the framework of precipitated clotted peloidal micrite and aragonite fibrous crystals forming spherulites. Primary voids in the carbonates are lined by fibrous aragonite cement forming isopachous rims (20–50 μm thick). EDS and XRD analyses confirm a predominant aragonite mineralogy with relatively minor percentages of calcite and dolomite within the carbonates as in previous studies.

Botryoidal and spherulitic aragonite of random orientation occur within the clotted micrite and are distinguished from surrounding micrite by larger crystal sizes and lighter color (**Figures 6B–D**). Gradual and irregular boundaries are observed between the botryoidal and spherulitic aragonite and the micrite (**Figures 6B–D**). The botryoidal and spherulitic aragonite have a patchy distribution and a negative correlation in abundance with the co-existing micrite. Under SEM, the botryoidal and spherulitic aragonite (10–30 μm in diameter) typically consist of fibrous crystals that radially fringe their irregular micritic nuclei (5–30 μm in diameter) (**Figure 6C**). The euhedral fibrous aragonite crystals are tightly packed and have blunt terminations, whereas the associated micritic nuclei consist of numerous spheroidal nanocrystals (100–700 nm in diameter) (**Figures 6A,C,D**). Additionally, microbial biofilm
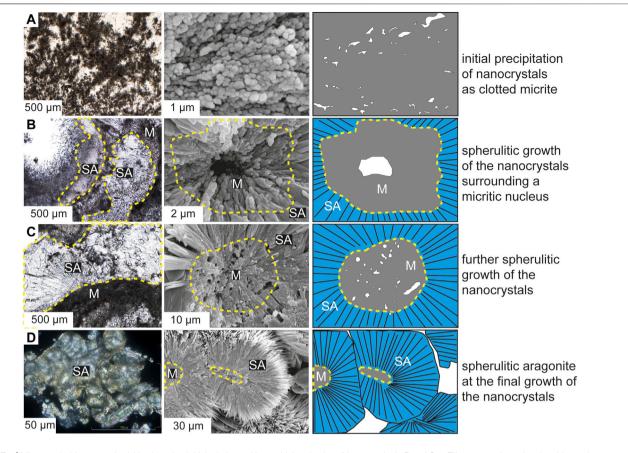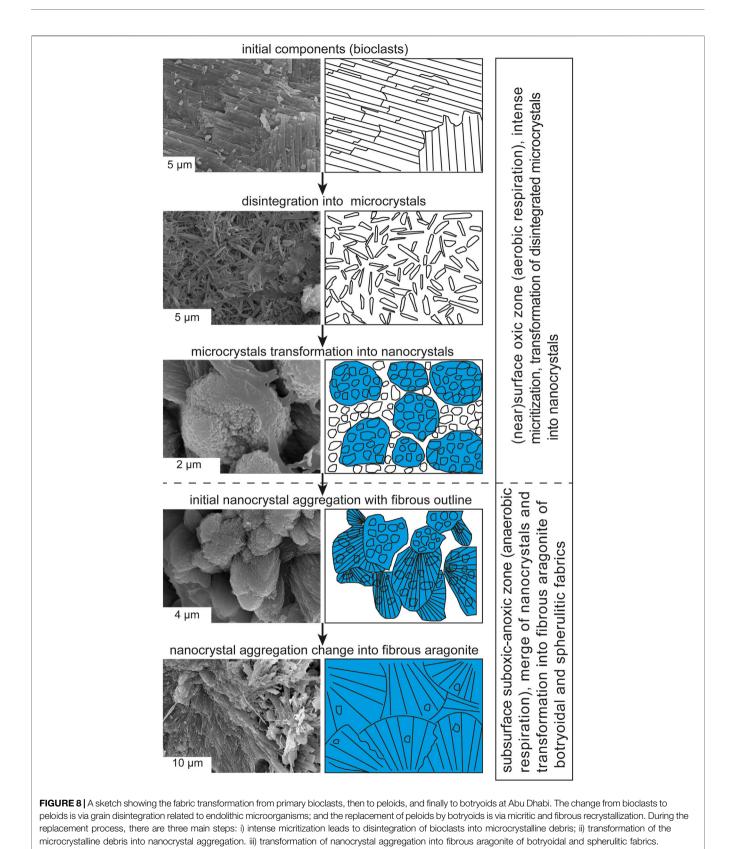
FIGURE 7 | Micro-scaled features of calcitic clotted peloidal micrite and botryoidal and spherulitic aragonite in Bagni San Filippo travertines showing thin section image **(left)**, SEM image **(middle)** and sketch **(right)**. M-micrite, SA-spherulitic aragonite. In **(A)**, the calcitic clotted peloidal micrite consisting of nanocrystals and forming most of the travertine fabrics. In **(B)**, aragonite fibers forming botryoidal and spherulitic structures nucleate on micritic substrate. The spherulite nucleus consists of a pore space with aragonitic nanocrystals with a radial fibrous arrangement grading outward into the fibrous crystals. In **(C)**, in the thin section photo on the left the contact between the calcitic micritic travertine and the fibrous aragonite crystal fans is sharp; under SEM, aragonite fibers, in a closely spaced radial arrangement, appear gradually transitional into aragonitic nanocrystals forming a porous framework at the nucleus. In **(D)**, aragonite spherulites form aggregated structures; under SEM spherulites consist of fibrous aragonite crystals with reduced to absent nanocrystals at the nuclei.
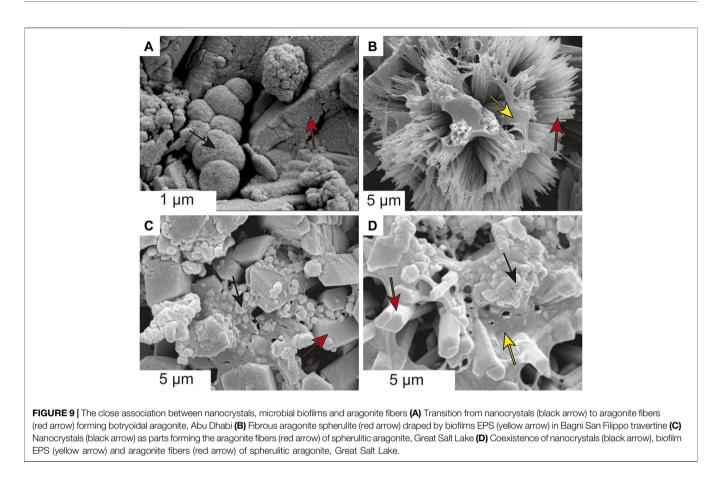
EPS is commonly associated with the botryoidal and spherulitic aragonite and micritic carbonate fabrics, possibly representing degraded microbial mats.

The water chemistry is characterized by high salinity, Mg/Ca ratio and aragonite supersaturation (**Table 1**). Isotope analyses of the carbonates yield $\delta^{13}C$ values from 2.8 to 5.6‰ and $\delta^{18}O$ values from −6.0 to −4.5‰. The $\delta^{13}C_{carb}$ (2.9–4.2‰) and $\delta^{18}O_{carb}$ (−6.0 to −4.7‰) values of gray clotted micrite fabrics are typically lower than the lighter color, spherulitic fabrics ($\delta^{13}C_{carb}$ = 4.3–5.6‰; $\delta^{18}O_{carb}$ = −5.4 to −4.5‰).

Botryoidal and Spherulitic Aragonite in the Hydrothermal Travertine of Bagni San Filippo

At Bagni San Filippo, dominantly calcitic travertine deposits contain fibrous aragonite crystals (0.9 to 1 mm in length) forming spherulites and botryoids only within the first few meters adjacent to the hydrothermal vent where water temperatures exceed 44°C. Carbonate precipitated from

thermal water coats microbial filaments (bacterial streamers *sensu* Farmer, 2000), gas bubbles and plant remains. In thin sections, the travertine consists mainly of clotted peloidal micrite (**Figure 7A**) and sparse fibrous spherulites (**Figures 7B–D**). The XRD analyses show a mixture of aragonite and calcite mineralogies. Other non-carbonate components include gypsum, and pyrite (**Table 1**). Under thin section, botryoidal and spherulitic aragonite show random orientation (**Figure 7B**), form fans and botryoids nucleating on the calcitic clotted peloidal micrite with a relatively sharp boundary (**Figure 7C**), or form clusters of spherulites with undulous extinction (**Figure 7D**). Under SEM, the clotted micrite consists of numerous spheroidal nanocrystals (100–600 nm in diameter) (**Figure 7A**) and shows microporosity and coexistence with microbial biofilm EPS. Radially oriented fibrous crystals form spherulites (10–300 μm in diameter) with a central nucleus either porous (**Figure 7B**) and/or made of spheroidal nanocrystals (**Figures 7B–D**), showing a gradual transition into the fibrous crystal. The portions of the fibrous aragonite crystals adjacent to the nuclei made of nanocrystals appear as formed by nanocrystal

FIGURE 8 | A sketch showing the fabric transformation from primary bioclasts, then to peloids, and finally to botryoids at Abu Dhabi. The change from bioclasts to peloids is via grain disintegration related to endolithic microorganisms; and the replacement of peloids by botryoids is via micritic and fibrous recrystallization. During the replacement process, there are three main steps: i) intense micritization leads to disintegration of bioclasts into microcrystalline debris; ii) transformation of the microcrystalline debris into nanocrystal aggregation. iii) transformation of nanocrystal aggregation into fibrous aragonite of botryoidal and spherulitic fabrics.

FIGURE 9 | The close association between nanocrystals, microbial biofilms and aragonite fibers **(A)** Transition from nanocrystals (black arrow) to aragonite fibers (red arrow) forming botryoidal aragonite, Abu Dhabi **(B)** Fibrous aragonite spherulite (red arrow) draped by biofilms EPS (yellow arrow) in Bagni San Filippo travertine **(C)** Nanocrystals (black arrow) as parts forming the aragonite fibers (red arrow) of spherulitic aragonite, Great Salt Lake **(D)** Coexistence of nanocrystals (black arrow), biofilm EPS (yellow arrow) and aragonite fibers (red arrow) of spherulitic aragonite, Great Salt Lake.

aggregations with a fibrous outline, which gradually transform away from the nuclei into euhedral fibrous crystals typically with squared terminations (**Figures 7B,C**).

The water properties (**Table 1**) show high temperature, high alkalinity, low Mg/Ca ratio and aragonite supersaturation. Bulk isotope analyses of the travertine samples show $\delta^{13}C_{carb}$ values from 4.8 to 5.9‰ and $\delta^{18}O_{carb}$ values from −12.6 to −12.1‰. Among the travertine fabrics, carbonate encrusted streamers have lower $\delta^{13}C_{carb}$ values (4.8–4.9‰) and similar $\delta^{18}O_{carb}$ values (−12.4 to −12.5‰) relative to coated gas bubbles and rafts ($\delta^{13}C_{carb} = 5.0$–5.9‰; $\delta^{18}O_{carb} = −12.6$ to −12.1‰).

INTERPRETATION AND DISCUSSION

Formation Process From Micritic Nuclei to Botryoidal and Spherulitic Aragonite

The botryoidal and spherulitic aragonite shown from the three cases described here generally fringe micritic "nuclei" or remnant fabrics (**Figure 4**; **Figure 6** and **Figure 7**). The nuclei seemingly provide a substrate for the botryoidal and spherulitic aragonite to develop. However, the nuclei shown here differ from the more common well-defined nuclei of many ooids and oncoids (Sandberg, 1975; Diaz et al., 2014; Pederson et al., 2015). In these more common types, the nuclei provide a substratum upon which carbonate needles accumulate. In contrast, in the examples shown here it is common to observe the

growth of botryoidal and spherulitic aragonite into, and at the expense of, the micritic nuclei, forming an inversion relationship between their volumetric abundance. Two formation pathways are interpreted from micritic nuclei to botryoidal and spherulitic aragonite in this study.

In the Abu Dhabi case setting, the formation process of botryoidal and spherulitic aragonite commences with micritization of grains (eventually forming micritic nuclei) (**Figure 4A**). Intense micritization by endolithic microorganisms leads to fabric destruction of bioclasts and their alteration to peloids, followed by disintegration of the peloids into skeletal needles and rods, which are bound by biofilms (**Figure 4B**; Ge et al., 2020b). Subsequently, these skeletal needles and rods transform into aggregations of spheroidal nanocrystals (**Figure 8**) associated with biofilms. Fibrous crystals of botryoidal and spherulitic aragonite then grow from these spheroidal nanocrystals (**Figure 8**), leading to irregular and indented contacts between fibrous crystals and nanocrystal aggregations (**Figures 4C,D**). During the initial growth stage, the fibrous crystals are present as nanocrystal aggregates with a fibrous outline (**Figure 9A**), but become euhedral crystals forming fan-like or spheroidal fabrics during subsequent growth. An inverse relation between the micritic nuclei size and the degree of fibrous crystal development is observed. During the formation of botryoidal and spherulitic aragonite, the encased nuclei show a progression from peloid relics consisting of skeletal rods and needles to aggregation of

spheroidal nanocrystals. Possible steps during this progression may include: 1) the skeletal rods and needles consist of nanocrystals within organic envelopes; 2) decomposition of the organic envelopes by microbial processes causes the breakdown of skeletal rods and needles to nanocrystals (Reid and MacIntyre, 1998; Stolarski and Mazur, 2005). Similar phenomena, referred to as "syn-depositional recrystallization," have been widely observed in tropical shallow marine carbonates in Florida, the Bahamas, and Belize (Reid et al., 1992; Reid and MacIntyre, 1998).

In the Great Salt Lake bioherm and Bagni San Filippo travertine case examples, the formation processes of botryoidal and spherulitic aragonite are thought to be primary mineral precipitation formed by aggregation of aragonite spheroidal nanocrystals (**Figure 6** and **Figure 7**). In case of the Great Salt Lake bioherms, the micritic nuclei of aragonitic spherulites have irregular outlines, and consist of numerous spheroidal nanocrystals associated with microbial biofilm EPS, independent of the degree of botryoidal and spherulitic aragonite development (**Figures 6C,D**). Over time, the micritic nuclei are reduced in size as the botryoidal and spherulitic aragonites grow toward the interiors of the micritic nuclei (**Figure 6**). The crystal growth of botryoidal and spherulitic aragonite toward the interiors of the micritic nuclei is evidenced by: 1) an inverse relationship in volumetric abundance between botryoidal and spherulitic aragonite and associated micrite nuclei, (e.g. **Figures 4C–E**); 2) gradual and irregular contact between botryoidal and spherulitic aragonite and associated micrite nuclei, (e.g. **Figures 4C–E**; **Figure 6** and **Figure 7**); 3) under SEM, the micritic nuclei are made of nanocrystals, and the terminations of botryoidal and spherulitic aragonite crystals toward the micritic nuclei consist of nanocrystal aggregations, with a gradual fabric transition between both, (e.g. **Figures 7B,C** and **Figure 9A**). In the case of the Bagni San Filippo travertine, the contact between the calcitic travertine, primarily composed of clotted peloidal micrite, and fibrous aragonite botryoids and fans appears sharp under petrographic observation (**Figure 7C**). Under SEM, fibrous aragonitic spherulites show nuclei with circular porous spaces and aragonitic nanocrystals that aggregate, gradually changing outward into euhedral fibrous crystals (**Figures 7B–D**).

In both Great Salt Lake bioherm and Bagni San Filippo travertine spherulites, progressing from the micritic nuclei made of nanocrystals outward to the fibrous aragonite crystals, a series of fabric transitions are observed from nanocrystal aggregations with random arrangement, to nanocrystal aggregation to mimic the shape of fibrous crystals, and finally to euhedral fibrous crystals without nanocrystals (**Figures 6B–D**; **Figures 7B–D** and **Figures 9B–D**).

The different formation mechanisms described above all include the formation and subsequent transformation of nanocrystals into fibrous botryoidal and spherulitic aragonite crystals. Similar formation processes, from nanocrystals to fibrous crystals with a radial arrangement, are common during the formation of marine invertebrate hardparts, (e.g. corals and mollusks; Stolarski and Mazur, 2005; Holcomb et al., 2009; Cohen and Holcomb, 2015) and have also been described in terrestrial spring carbonates (Pedley, 2014; Jones, 2017a, Jones, 2017b; Franchi and Frisia, 2020).

Formation Mechanisms of Botryoidal and Spherulitic Aragonite: Replacement and Precipitation

The botryoidal and spherulitic aragonites from Abu Dhabi are likely early recrystallization (replacement) products of peloids (representing micritized bioclasts). An interpreted replacement origin is based on the following petrographic characteristics: 1) irregular and transitional contacts between the botryoidal and spherulitic aragonite and the associated relict peloid nuclei; 2) distribution of the botryoidal and spherulitic aragonite within the interiors of peloid components; 3) an inverse relationship in spatial abundance of botryoidal or spherulitic aragonite and coexisting peloids; 4) local occurrence of early marine cement surrounding the botryoidal and spherulitic aragonite; and 5) abundant inclusions in the botryoidal and spherulitic aragonite (**Figure 4** and **Figure 5**). Moreover, triple enfacial junctions, appearing in thin section as darker sutures, are often present at the contact zones between adjacent botryoids and spherulites (**Figure 5C**), evidencing a replacement process (Warren, 1982). Additional evidence for a replacement origin comes from characteristics of microborings within the botryoidal and spherulitic aragonite. The microborings have sharp and regular surfaces and occur within fibrous botryoidal and spherulitic aragonite crystals. Fragments of botryoidal and spherulitic aragonite within the microborings are lacking (**Figure 5F**). Microborings within the botryoidal and spherulitic aragonite are similar in terms of size and morphology to those within the peloids (**Figures 5E,F**). In the view of the authors, the microboring features enclosed within the botryoidal and spherulitic aragonite are inherited from former peloids, (i.e. older than the formation of the replacement aragonite) and are preserved as ghost structures during the replacement process. Additional evidence for this replacement is the absence of comparable microborings in the interstitial early marine cements (**Figure 5H**).

In the case of Great Salt Lake and Bagni San Filippo, the botryoidal and spherulitic aragonites are considered of primary precipitation origin, formed by aggregation of nanocrystal precipitates. Under SEM, the nanocrystal precipitates are evidenced by relatively uniform size and morphology and no association or relation with allochthonous skeletal debris. The origin as primary precipitates for these two cases is supported by supersaturated water properties (**Table 1**) and is consistent with former studies (Folk, 1994; Pentecost, 1995, 2005; Della Porta, 2015; Pace et al., 2016; Della Porta et al., 2017a, Della Porta et al., 2017b; Lindsay et al., 2017).

In the three case studies, the change in crystal size and morphology from nanocrystals to botryoidal and spherulitic fabrics may be driven by: 1) thermodynamic processes referred to as "Ostwald ripening," where smaller crystals dissolve and reprecipitate as larger crystals with the same mineralogy in order to reduce free surface energy (Ostwald, 1897; Kirkland et al., 1999; Franchi and Frisia, 2020); 2) high Mg/Ca ratios favoring fibrous

growth (Folk, 1974, 1994; Jones, 2017a, Jones, 2017b); and 3) decreasing organic components from nanocrystals to fibrous crystals (Stolarski and Mazur, 2005). In summary, the botryoidal and spherulitic aragonite in this study are formed via replacement (Abu Dhabi) or primary precipitation via aggregation of nanocrystal aragonite precipitates (Bagni San Filippo and Great Salt Lake).

Botryoidal and Spherulitic Aragonite Associated with Microbial Mats

Despite the supersaturated water, with respect to aragonite, in the three case studies discussed here (**Table 1**), the presence of microbial mats and biofilm EPS closely associated with the investigated fibrous aragonites indicates a possible microbially mediated influence in their formation.

The botryoidal and spherulitic aragonite of Abu Dhabi show different environmental features relative to typical marine fibrous aragonite cements. In the Abu Dhabi coastal area and other places in the southwestern Persian Gulf, typical fibrous aragonite cements are common due to widespread early marine cementation (Shinn, 1969; Paul and Lokier, 2017; Ge et al., 2020a, Ge et al., 2020b). These typical marine cements are characterized by: 1) various sizes and morphologies in intergranular pores; 2) competitive growth, intercrystal porosity, and lack of nanocrystals in composition; 3) dominance in the lagoonal and open marine settings where botryoidal and spherulitic aragonite are very scarce (Shinn, 1969; Paul and Lokier, 2017; Ge et al., 2020a, Ge et al., 2020b). Whereas typical fibrous marine cements show ubiquitous formation in the shallow marine realm, botryoidal and spherulitic aragonites are only abundant in the intertidal microbial mats. The petrological and environmental differences of these cement types provide evidence for specific factors for the formation of botryoidal and spherulitic aragonite, apart from aragonite-saturated seawater. The close association between microbial mats and botryoidal and spherulitic fabrics in Abu Dhabi indicates an influence of the abundant microbial biofilm EPS.

In the case of the Bagni San Filippo travertines and the Great Salt Lake bioherms, the botryoidal and spherulitic aragonites also show a close relation with microbial mats. The nanocrystals, nanometer-size carbonate, changing into botryoidal and spherulitic aragonite also develop microporosity, and show association with EPS (**Figures 9B–D**), indicating a possible influence by the presence of biofilm substrates and/or microbial mediation (Folk, 1994; Chafetz and Guidry, 1999; Riding, 2000, Riding, 2008; Pentecost, 2005; Della Porta, 2015; Pace et al., 2016). The influence of microbial mats on botryoidal and spherulitic aragonite is also supported by precipitation experiments producing similar nanocrystals in organic-rich environments (Kirkland et al., 1999). However, the abiotic and biologically induced and influenced processes driving carbonate precipitation seem different in the subaerial hydrothermal system of the travertines and hypersaline lacustrine setting of the bioherms.

In the case of Bagni San Filippo, travertine deposits form at the subaerial emergence of hydrothermal fluids at high temperatures, with carbonate precipitation primarily driven by physico-

chemical processes such as CO_2 degassing (Folk, 1994; Pentecost, 2005; Capezzuoli et al., 2014; Della Porta, 2015; Della Porta et al., 2017a, Della Porta et al., 2017b, Della Porta et al., 2021 and references therein). In the central Italian hydrothermal settings, primary carbonate precipitation is favored by sufficient Ca^{2+} and CO_3^{2-} in thermal waters derived from decarbonation reactions with the Mesozoic carbonate substrate (Minissale, 2004). Travertines are mostly calcitic, with aragonite precipitates only occurring at temperatures >40°C (Folk, 1993, 1994). In Bagni San Filippo, aragonite spherulites are only observed associated with the calcitic travertine fabrics near the vent at temperatures >44°C. Higher temperatures will favor aragonite precipitation (Folk, 1994; Jones, 2017b). Furthermore, higher temperatures (>44°C) and closer location to vents may facilitate rapid CO_2 degassing and higher saturation levels, further promoting aragonite precipitation (cf. Jones, 2017b). Microbial mats are also ubiquitous in such high temperature environments and part of the travertine precipitates may be biologically influenced (cf. Dupraz et al., 2009), with EPS or other organic matter acting as a substrate for mineral precipitation (Folk, 1993, 1994; Chafetz and Guidry, 1999; Riding, 2008; Jones and Peng, 2012, Jones and Peng, 2014; Della Porta, 2015; Della Porta et al., 2017a, Della Porta et al., 2021). Although the existence of microbes may enhance CO_2 degassing, the influence of microbial biofilms and/or EPS on travertine mineralogies (calcite vs. aragonite) is difficult to assess, as it may change at scales <1 μm (Jones, 2017b). In the case of Great Salt Lake, Pace et al. (2016) proposed that the microbial bioherm formation is linked to microbial metabolisms via the following processes: 1) a Mg-Si phase forms on the EPS due to increased pH driven by cyanobacteria photosynthesis; 2) aragonite nucleates following cyanobacteria biofilm degradation by sulfate-reducing bacteria with intestine-like aragonite (as Pace et al., 2016 label the spherulitic aragonite) nucleating inside coccoid clusters, expanding in the extracellular organic matrix and embedding the Mg-Si phases; 3) dolomite partially replaces aragonite in neutral to acidic pore water by dissolution-reprecipitation reactions. Sulfate-reducing bacteria may play a fundamental role for the nucleation and growth of aragonite crystals (Pace et al., 2016) and dolomite formation (Dunham et al., 2020). Lindsay et al. (2017) proposed that bioherm carbonate precipitation is instead primarily mediated by cyanobacteria photosynthesis.

In at least some of the case settings studied here, the botryoidal and spherulitic aragonite seem to form under reducing porewater conditions rich in organic material. This is supported by the association of an H_2S odor, black sediment, and pyrites in the Abu Dhabi microbial mats. Pyrites were observed in the Great Salt Lake bioherm carbonates, often appearing dark gray in color at a few centimeters below the top microbial mat (**Table 1**; **Figure 2**). Sulfate reduction was proposed as the key precipitation mechanism for the Great Salt Lake microbial bioherms by Pace et al. (2016). Similar nanocrystals as described in this study were also interpreted to be formed in associated with EPS degradation and sulfate reduction in anoxic zones below the microbial mat surface (Dupraz et al., 2004; Pace et al., 2016). This interpretation is consistent with the Great Salt Lake and Abu

Dhabi case examples, where the nanocrystals occur in close association with biofilms beneath the mat surfaces. Anaerobic microbial activity in these settings is possibly related to organic decay, resulting in increased alkalinity (Grotzinger and Knoll, 1995; Dupraz et al., 2009; Pace et al., 2016). A relation between high seawater alkalinity and anaerobic microbial activity is supported by the fact that in the Abu Dhabi coastal area, the intertidal microbial mats have higher seawater pH and alkalinity relative to other settings (Ge et al., 2020a). Evidence comes from anoxic settings elsewhere. Goyet et al. (1991) reported that microbial processes can induce 3–4 times higher carbonate alkalinity values in interstitial water compared to open and oxic marine settings at similar depths. Based on these considerations, the formation (or simply the rate of precipitation) of botryoidal and spherulitic aragonite may be linked in some cases, as in the Abu Dhabi intertidal microbial mats and in the Great Salt Lake microbial bioherms, to high porewater alkalinity induced by microbial activity in reducing and organic-rich conditions. Moreover, microbial EPS may serve as substrates for calcium carbonate precipitation (Dupraz et al., 2009). Despite the microbially mediated influence on the studied fabrics, care must be taken to not oversimplify the formation processes. The exceptionally complex nature of microbe-carbonate mineral reactions in the presence of microbial consortia (Riding, 2000; Dupraz et al., 2009 and references therein) likely imply that the boundaries between biologically induced and -influenced mineralization on carbonates in the presence of microbes are often not obvious.

Distinction of Botryoidal and Spherulitic Aragonite of Different Origins and Paleoenvironmental Significance

Previous studies often described mm-to m-scale botryoidal and spherulitic aragonite in various depositional settings formed as precipitates from marine or non-marine waters, (e.g. Ginsburg and James, 1976; Taviani and Rabbi, 1984; Grotzinger and Kasting, 1993; van der Kooij et al., 2010; Jones, 2017a, b and references therein). In contrast, this study documents that both, replacement and precipitation processes may induce the formation mechanisms of µm to mm-scale botryoidal and spherulitic aragonite in carbonate settings associated with microbial mats and microbialite formation. We propose that further research must focus on the question to which degree the µm to mm-scale botryoidal and spherulitic aragonite described here are, beyond similarities in terms of their fabric, comparable to the often much larger aragonites in reefal framework cavities, (e.g. Ginsburg and James, 1976; Aissaoui, 1985).

Botryoidal and spherulitic aragonite in reefal cavities (up to 1 m in size) generally grow in open voids as marine precipitates with oriented distribution, and are often associated with internal sediment, (e.g. Ginsburg and James, 1976; Aissaoui, 1985). The botryoidal and spherulitic aragonite described herein, however, are characterized by their small (µm to mm) size, random orientation, and growth within micritic (both micritic sediment and precipitated clotted peloidal micrite) host

sediments. Another probable difference is the formation process of fibrous crystals of botryoidal and spherulitic aragonite. The fibrous crystals in open-marine, metazoan-reefal cavities are generally not derived from micritic nuclei and grow toward free pore space. Instead, the fibrous crystals in the carbonate settings studied herein are formed via aggregation of nanocrystals, are controlled by micritic nuclei, and seem to grow toward the interiors of associated micrite.

Based on this and previous studies, petrological criteria are proposed here to distinguish different formation processes of botryoidal and spherulitic aragonite. Botryoidal and spherulitic aragonite with a replacement-origin are characterized by: 1) random distribution within peloidal micrite, (e.g. **Figure 5A**); 2) gradual and irregular contacts with associated micrite, (e.g. **Figure 5A**); 3) an inverse relationship in spatial abundance with associated micrite, (e.g. **Figure 4**), 4) growth toward the interiors of associated micrite, (e.g. **Figure 4**); 5) allochthonous origin for associated micrite with different sizes and morphologies, (e.g. skeletal rods and needles; **Figure 4B**); 6) cross cutting, (e.g. **Figure 5D**) or inheriting former fabrics, (e.g. **Figures 5B,E,F**); and 7) abundant micritic inclusions, (e.g. **Figures 5A,C**).

Botryoidal and spherulitic aragonite primary precipitates formed via aggregation of nanocrystals associated with organic substrates provided by microbial mats may show: 1) random distribution within peloidal micrite, (e.g. **Figure 6**); 2) gradual or irregular contacts with associated micrite, (e.g. **Figure 6**); 3) an inverse relationship in spatial abundance with associated micrite nuclei, (e.g. **Figure 6** and **Figure 7**), 4) growth toward the interiors of associated micrites, (e.g. **Figure 6** and **Figure 7**); 5) associated micrites mainly consisting of nanocrystals of autochthonous origin with relatively similar size and morphology, (e.g. **Figure 6** and **Figure 7**); and 6) lack of allochthonous micrite such as skeletal debris in the associated micrites, (e.g. **Figure 6** and **Figure 7**).

In contrast, botryoidal and spherulitic aragonite formed as abiotic precipitates are characterized by: 1) oriented distribution within the pore system and growth toward free pore space, (e.g. Ginsburg and James, 1976); 2) relatively regular and sharp contact with the substrates of precipitation, (e.g. Taviani and Rabbi, 1984); 3) no inverse relationship in spatial abundance with micritic nuclei, (e.g. Aissaoui, 1985); and 4) coexistence with other kinds of early precipitates (and microbial carbonates) in the pore system such as fibrous calcite, (e.g. van der Kooij et al., 2010).

Implications for Ancient Analogues and Paleoenvironmental Significance

The recognition of different origins for botryoidal and spherulitic aragonite has important paleoenvironmental implications. Geologically, in the Archean and Paleoproterozoic, abundant botryoidal and spherulitic aragonite and similar aragonite fabrics, (e.g. crystal fans) associated with microbialites occurred as cavity fillings and seafloor crusts within marine settings (Grotzinger and Knoll, 1995; Sumner and Grotzinger, 2000; Riding, 2008). In the Phanerozoic, botryoidal and spherulitic aragonite mainly occur during the "aragonite seas" of the (sub)tropical realm (Sandberg, 1983), such as in the

Pennsylvanian, late Permian and Early to Middle Triassic (Mazzullo, 1980; Sandberg, 1983, 1985; Grotzinger and Knoll, 1995; Russo et al., 1997; Wood, 1999; Della Porta et al., 2003; Pruss et al., 2006; van der Kooij et al., 2010). These ancient botryoidal and spherulitic aragonites, typically interpreted as direct marine precipitates, associated with other marine fabrics and ooids, have been used to infer seawater oscillations between aragonite seas and calcite seas (Sandberg, 1983, 1985). Remarkably, in the Archean and Paleoproterozoic and the Carboniferous to Middle Permian as well as the late Permian to Middle Triassic, abundant marine botryoidal and spherulitic aragonite are characterized by: 1) close association with considerable microbialites; and 2) constituent parts of bulk sediment rather than pore-infillings (Grotzinger and Knoll, 1995; Sumner and Grotzinger, 2000; Pruss et al., 2006; Riding, 2008). These features are more similar to this study. If the concepts of diverse origins discussed here are of value for their ancient analogues, then it would be worth testing if some of the ancient botryoidal and spherulitic aragonites possibly have an early replacement origin. These considerations have clear implications in paleoceanography and carbonate research.

Elemental and isotope data of marine botryoidal and spherulitic aragonite precipitates appear to record, within the limitations of fluid-mineral disequilibrium precipitation processes (Swart, 2015), ambient seawater signatures, (e.g. Ginsburg and James, 1976; Taviani and Rabbi, 1984). In the Abu Dhabi case example featuring replacement botryoidal and spherulitic aragonites, the translation of proxy data to seawater properties is, depending on the final preserved mineralogy and origin of the precursor phase, more complex (Sandberg, 1985). Furthermore, when botryoidal and spherulitic aragonite are formed in association with microbial biofilm EPS, the type and degree of influence of organic substrates during their formation and porewater-carbonate fractionation patterns possibly differ from the typically inorganic precipitates as observed in recent reefal settings, (e.g. Ginsburg and James, 1976; Taviani and Rabbi, 1984). The difference is supported by relatively lower $\delta^{13}C_{carb}$ values at Abu Dhabi compared to recent reefal settings (Ginsburg and James, 1976; Taviani and Rabbi, 1984). Isotope data of Bagni San Filippo and Great Salt Lake carbonates record: 1) a 1–3‰ difference between maximum and minimum $\delta^{13}C_{carb}$ values in different precipitated micrite fabrics containing botryoidal and spherulitic aragonite; and 2) micrite fabrics with higher organic content, indicated by darker color and/or increased abundance of biofilm EPS, show relatively lower $\delta^{13}C_{carb}$ values. The interaction and relative importance between organic and inorganic factors should therefore be considered when interpreting geochemical data of botryoidal and spherulitic aragonite. In addition, the replacement mechanism by which micrites transform into fibrous crystals in the Abu Dhabi case example may provide a new diagenetic pathway of recrystallization from micrite to microspar during early marine diagenesis. The recrystallization pattern differs from previously proposed recrystallization models, such as those discussed in Shinn (1969), Loucks and Folk (1976), Longman (1980), and Munnecke et al. (1997).

CONCLUSION

Three present-day case examples of μm to mm-scale botryoidal and spherulitic aragonite associated with microbial mats are documented here. These include intertidal microbial mats in Abu Dhabi, microbial bioherms in the Great Salt Lake, and hydrothermal travertines in Bagni San Filippo. Based on petrographic characterization, the botryoidal and spherulitic aragonite consist of radially oriented fibrous crystals, and generally surround micritic nuclei. Different formation mechanisms of these fabrics are proposed: 1) replacement at Abu Dhabi; and 2) primary formation through aggregation of nanocrystal precipitates at Great Salt Lake and Bagni San Filippo. At Abu Dhabi, intense micritization leads to disintegration of former aragonitic bioclasts into skeletal rods and needles. These rods and needles are subsequently recrystallized into spheroidal nanocrystals, which grow into fibrous crystals of botryoidal and spherulitic aragonite. At Great Salt Lake and Bagni San Filippo, spheroidal aragonite nanocrystals are initially precipitated in association with microbial biofilms, and subsequently grow into fibrous crystals of botryoidal and spherulitic aragonite via aggregation. The nanocrystals from all localities are closely associated with biofilms, and their formation in Abu Dhabi intertidal microbial mats and Great Salt Lake bioherms may be related to increased alkalinity due to microbial activity associated with organic degradation in oxygen-limited environments. In Bagni San Filippo, travertine deposits are dominated by calcite but sparse aragonitic spherulites form on microbial biofilms in EPS substrates at temperatures higher than 44°C near the vent. This seems indicative of a primary physico-chemical factor driving aragonite precipitation. Compared with botryoidal and spherulitic aragonite formed by marine precipitation in open-marine reefal cavities, the botryoidal and spherulitic aragonite discussed here have different formation mechanisms and spatial distribution, making the comparability of these fabrics unclear at present. In the view of the authors, the recognition of different botryoidal and spherulitic aragonite types is highly relevant for those concerned with paleoenvironmental research.

DATA AVAILABILITY STATEMENT

The original contributions presented in the study are included in the article/**Supplementary Material**, further inquiries can be directed to the corresponding authors.

AUTHOR CONTRIBUTIONS

YG analyzed the data and wrote the initial manuscript with GP, CP, and AI. GP, CP, SL, RH, and AI assisted with data collection and analysis, and provided instructions and feedback on the manuscript. All authors contributed to the article and approved the submitted version.

ACKNOWLEDGMENTS

SUPPLEMENTARY MATERIAL

The Supplementary Material for this article can be found online at: https://www.frontiersin.org/articles/10.3389/feart.2021.698952/full#supplementary-material

SUPPLEMENTARY FIGURE 1 | EBSD analysis of spherulitic fabrics from Abu Dhabi, confirming the aragonite mineralogy. (A) Spherulitic aragonite in thin section.

(B) Spherulitic aragonite (same to Figure A) under SEM. (C) Mineralogy map of Figure B, showing dominantly aragonite for both spherulitic aragonite and associated micritic nuclei. (D) Crystal fabric map of Figure B, showing gradual transition between micritic nuclei (smaller crystal size, red color) to aragonite fibers (larger crystal size, green or blue color).

SUPPLEMENTARY FIGURE 2 | Thin section scans of samples containing botryoidal and spherulitic aragonite. (A) Firmground sample from Abu Dhabi microbial carbonates. (B) Sample of Great Salt Lake microbial bioherm showing the porous framework consisting of clotted peloidal micrite and spherulitic aragonite fabric. (C) Bagni San Filippo travertine sample showing the laminated porous streamer fabric.

SUPPLEMENTARY FIGURE 3 | Microphotographs of botryoidal and spherulitic aragonite. (A) Botryoidal and spherulitic aragonite (indicated by red arrow) in the carbonate firmgrounds associated with microbial mats at Abu Dhabi. (B) Botryoidal and spherulitic aragonite (indicated by red arrows) in Abu Dhabi microbial carbonates. (C) Botryoidal and spherulitic aragonite (indicated by red arrow) associated with clotted peloidal micrite forming the bulk framework of the microbial bioherms at Great Salt Lake. (D) Image in crossed polarizers of botryoidal and spherulitic aragonite (indicated by red arrows) comprised within the clotted peloidal micrite forming the microbial bioherms at Great Salt Lake. (E) Botryoidal and spherulitic aragonite (indicated by red arrow) in travertine deposits at Bagni San Filippo. (F) Botryoids of fibrous aragonite (indicated by red arrows) nucleating on laminated clotted peloidal micrite framework in travertine deposits at Bagni San Filippo.

REFERENCES

Aissaoui, D. M. (1985). Botryoidal Aragonite and its Diagenesis. *Sedimentology* 32, 345–361. doi:10.1111/j.1365-3091.1985.tb00516.x

Allen, C., Albert, F. G., Chafetz, H. S., Combie, J., Graham, C. R., Kieft, T. L., et al. (2000). Microscopic Physical Biomarkers in Carbonate hot springs: Implications in the Search for Life on Mars. *Icarus* 147, 49–67. doi:10.1006/icar.2000.6435

Anbar, A. D., Duan, Y., Lyons, T. W., Arnold, G. L., Kendall, B., Creaser, R. A., et al. (2007). A Whiff of Oxygen before the Great Oxidation Event? *Science* 317, 1903–1906. doi:10.1126/science.1140325

Bates, R. L., and Jackson, J. A. (1980). *Glossary of Geology*. 2nd Edition. Falls Church. Virginia: American Geological Institute.

Bathurst, R. G. C. (1966). Boring Algae, Micrite Envelopes and Lithification of Molluscan Biosparites. *Geol. J.* 5, 15–32.

Baxter, B. K. (2018). Great Salt Lake Microbiology: a Historical Perspective. *Int. Microbiol.* 21, 79–95. doi:10.1007/s10123-018-0008-z

Bekker, A., Holland, H. D., Wang, P.-L., Rumble, D., Stein, H. J., Hannah, J. L., et al. (2004). Dating the Rise of Atmospheric Oxygen. *Nature* 427, 117–120. doi:10.1038/nature02260

Bouton, A., Vennin, E., Boulle, J., Pace, A., Bourillot, R., Thomazo, C., et al. (2016). Linking the Distribution of Microbial Deposits from the Great Salt Lake (Utah, USA) to Tectonic and Climatic Processes. *Biogeosciences* 13, 5511–5526. doi:10.5194/bg-13-5511-2016

Brogi, A., and Fabbrini, L. (2009). Extensional and Strike-Slip Tectonics across the Monte Amiata-Monte Cetona Transect (Northern Apennines, Italy) and Seismotectonic Implications. *Tectonophysics* 476, 195–209. doi:10.1016/j.tecto.2009.02.020

Capezzuoli, E., Gandin, A., and Pedley, M. (2014). Decoding Tufa and Travertine (Fresh Water Carbonates) in the Sedimentary Record: the State of the Art. *Sedimentology* 61, 1–21. doi:10.1111/sed.12075

Carminati, E., and Doglioni, C. (2012). Alps vs. Apennines: the Paradigm of a Tectonically Asymmetric Earth. *Earth-Science Rev.* 112, 67–96. doi:10.1016/j.earscirev.2012.02.004

Carozzi, A. V. (1962). Observations on Algal Biostromes in the Great Salt Lake, Utah. *J. Geology* 70, 246–252. doi:10.1086/626814

Chafetz, H. S., and Folk, R. L. (1984). Travertines; Depositional Morphology and the Bacterially Constructed Constituents. *J. Sediment. Res.* 54, 289–316. doi:10.1306/212F8404-2B24-11D7-8648000102C1865D

Chafetz, H. S., and Guidry, S. A. (1999). Bacterial Shrubs, crystal Shrubs, and ray-crystal Shrubs: Bacterial vs. Abiotic Precipitation. *Sediment. Geology* 126, 57–74. doi:10.1016/S0037-0738(99)00032-9

Chidsey, T. C., Jr, Vanden Berg, M. D., and Eby, D. E. (2015). "Petrography and Characterization of Microbial Carbonates and Associated Facies from Modern Great Salt Lake and Uinta Basin's Eocene Green River Formation in Utah, USA," in *Microbial Carbonates in Space and Time: Implications for Global Exploration and Production*. Editors D. W. J. Bosence, K. A. Gibbons, D. P. Le Heron, W. A. Morgan, T. Pritchard, and B. A. Vining (Bath: Geological Society, London, Special Publications), 418, 261–286. doi:10.1144/sp418.6

Cohen, A., and Holcomb, M. (2009). Why Corals Care about Ocean Acidification: Uncovering the Mechanism. *Oceanog.* 22, 118–127. doi:10.5670/oceanog.2009.102

Colman, S. M., Kelts, K. R., and Dinter, D. A. (2002). Depositional History and Neotectonics in Great Salt Lake, Utah, from High-Resolution Seismic Stratigraphy. *Sediment. Geology* 148, 61–78. doi:10.1016/s0037-0738(01)00210-x

Croci, A., Della Porta, G., and Capezzuoli, E. (2016). Depositional Architecture of a Mixed Travertine-Terrigenous System in a Fault-Controlled continental Extensional basin (Messinian, Southern Tuscany, Central Italy). *Sediment. Geology* 332, 13–39. doi:10.1016/j.sedgeo.2015.11.007

Davies, G. R. (1977). Former Magnesian Calcite and Aragonite Submarine Cements in Upper Paleozoic Reefs of the Canadian Arctic: A Summary. *Geol.* 5, 11–15. doi:10.1130/0091-7613(1977)5<11:FMCAAS>2.0.CO;2

Della Porta, G., Capezzuoli, E., and De Bernardo, A. (2017a). Facies Character and Depositional Architecture of Hydrothermal Travertine Slope Aprons (Pleistocene, Acquasanta Terme, Central Italy). *Mar. Pet. Geology* 87, 171–187. doi:10.1016/j.marpetgeo.2017.03.014

Della Porta, G. (2015). "Carbonate Build-Ups in Lacustrine, Hydrothermal and Fluvial Settings: Comparing Depositional Geometry, Fabric Types and Geochemical Signature," in *Microbial Carbonates in Space and Time: Implications for Global Exploration and Production*. Editors D. W .J. Bosence, K. A. Gibbons, D. P. Le Heron, W. A. Morgan, T. Pritchard, and B. A. Vining (Bath: Geological Society, London, Special Publications), 418, 17–68. doi:10.1144/SP418.4

Della Porta, G., Croci, A., Marini, M., and Kele, S. (2017b). Depositional Architecture, Facies Character and Geochemical Signature of the Tivoli Travertines (Pleistocene, Acque Albule Basin, Central Italy). *RIPS Riv. Ital. Paleontol. Stratigr.* 123, 487–540. doi:10.13130/2039-4942/9148

Della Porta, G., Hoppert, M., Hallmann, C., Schneider, D., and Reitner, J. (2021). The Influence of Microbial Mats on Travertine Precipitation in Active Hydrothermal Systems (Central Italy). *Depositional Rec.*, 1–39. doi:10.1002/dep2.147

Della Porta, G., Kenter, J. A. M., Bahamonde, J. R., Immenhauser, A., and Villa, E. (2003). Microbial Boundstone Dominated Carbonate Slope (Upper Carboniferous, N Spain): Microfacies, Lithofacies Distribution and Stratal Geometry. *Facies* 49, 175–207. doi:10.1007/s10347-003-0031-0

Diaz, M. R., Van Norstrand, J. D., Eberli, G. P., Piggot, A. M., Zhou, J., and Klaus, J. S. (2014). Functional Gene Diversity of Oolitic Sands from Great Bahama Bank. *Geobiology* 12, 231–249. doi:10.1111/gbi.12079

Doglioni, C. (1991). A Proposal for the Kinematic Modelling of W-Dipping Subductions - Possible Applications to the Tyrrhenian-Apennines System. *Terra Nova* 3, 423–434. doi:10.1111/j.1365-3121.1991.tb00172.x

Duchi, V., Giordano, M. V., and Martini, M. (1978). Riesame del problema della precipitazione di calcite od aragonite da soluzione naturali. *Rend. Soc. Ital. Mineral. Petrol.* 34, 605–618.

Dunham, E. C., Fones, E. M., Fang, Y., Lindsay, M. R., Steuer, C., Fox, N., et al. (2020). An Ecological Perspective on Dolomite Formation in Great Salt Lake, Utah. *Front. Earth Sci.* 8, 24. doi:10.3389/feart.2020.00024

Dupraz, C., Reid, R. P., Braissant, O., Decho, A. W., Norman, R. S., and Visscher, P. T. (2009). Processes of Carbonate Precipitation in Modern Microbial Mats. *Earth-Science Rev.* 96, 141–162. doi:10.1016/j.earscirev.2008.10.005

Dupraz, C., Visscher, P. T., Baumgartner, L. K., and Reid, R. P. (2004). Microbe-mineral Interactions: Early Carbonate Precipitation in a Hypersaline lake (Eleuthera Island, Bahamas). *Sedimentology* 51, 745–765. doi:10.1111/j.1365-3091.2004.00649.x

Eardley, A. J. (1938). Sediments of Great Salt Lake, Utah. *AAPG* 22, 1305–1411.

Faccenna, C., Soligo, M., Billi, A., De Filippis, L., Funiciello, R., Rossetti, C., et al. (2008). Late Pleistocene Depositional Cycles of the Lapis Tiburtinus Travertine (Tivoli, Central Italy): Possible Influence of Climate and Fault Activity. *Glob. Planet. Change* 63, 299–308. doi:10.1016/j.gloplacha.2008.06.006

Farmer, J. D. (2000). Hydrothermal Systems: Doorways to Early Biosphere Evolution. *GSA Today* 10, 1–9.

Feng, D., Chen, D., and Roberts, H. H. (2008). Sedimentary Fabrics in the Authigenic Carbonates from Bush Hill: Implication for Seabed Fluid Flow and its Dynamic Signature. *Geofluids* 8, 301–310. doi:10.1111/j.1468-8123.2008.00231.x

Flügel, E. (2010). *Microfabrics of Carbonate Rocks*. Heidelberg: Springer.

Folk, R. (1994). Interaction between Bacteria, Nannobacteria, and mineral Precipitation in hot springs of central Italy. *Geogr. Phys. Quatern.* 48, 233–246.

Folk, R. L. (1959). Practical Petrographic Classification of Limestones. *AAPG* 43, 1–38.

Folk, R. L. (1993). SEM Imaging of Bacteria and Nannobacteria in Carbonate Sediments and Rocks. *J. Sediment. Res.* 63, 990–999. doi:10.1306/D4267C67-2B26-11D7-8648000102C1865D

Folk, R. L. (1974). The Natural History of Crystalline Calcium Carbonate: Effect of Magnesium Content and Salinity. *J. Sediment. Res.* 44, 40–53.

Ford, T. D., and Pedley, H. M. (1996). A Review of Tufa and Travertine Deposits of the World. *Earth-Science Rev.* 41, 117–175. doi:10.1016/s0012-8252(96)00030-x

Fouke, B. W. (2011). Hot-spring Systems Geobiology: Abiotic and Biotic Influences on Travertine Formation at Mammoth Hot Springs, Yellowstone National Park, USA. *Sedimentology* 58, 170–219. doi:10.1111/j.1365-3091.2010.01209.x

Franchi, F., and Frisia, S. (2020). Crystallization Pathways in the Great Artesian Basin (Australia) spring mound Carbonates: Implications for Life Signatures on Earth and beyond. *Sedimentology* 67, 2561–2595. doi:10.1111/sed.12711

Ge, Y., Lokier, S. W., Hoffmann, R., Pederson, C. L., Neuser, R. D., and Immenhauser, A. (2020b). Composite Micrite Envelopes in the Lagoon of Abu Dhabi and Their Application for the Recognition of Ancient Firm- to Hardgrounds. *Mar. Geology* 423, 106141. doi:10.1016/j.margeo.2020.106141

Ge, Y., Pederson, C. L., Lokier, S. W., Traas, J. P., Nehrke, G., Neuser, R. D., et al. (2020a). Late Holocene to Recent Aragonite-cemented Transgressive Lag Deposits in the Abu Dhabi Lagoon and Intertidal Sabkha. *Sedimentology* 67, 2426–2454. doi:10.1111/sed.12707

Ginsburg, R. N., and James, N. P. (1976). Submarine Botryoidal Aragonite in Holocene Reef Limestones, Belize. *Geol.* 4, 431–436. doi:10.1130/0091-7613(1976)4<431:SBAIHR>2.0.CO;2

Goyet, C., Bradshaw, A. L., and Brewer, P. G. (1991). The Carbonate System in the Black Sea. *Deep-sea Res.* 38, 1049–1068. doi:10.1016/0198-0149(10)80023-8

Grotzinger, J. P., and Kasting, J. F. (1993). New Constraints on Precambrian Ocean Composition. *J. Geology* 101, 235–243. doi:10.1086/648218

Grotzinger, J. P., and Knoll, A. H. (1995). Anomalous Carbonate Precipitates: Is the Precambrian the Key to the Permian?. *Palaios* 10, 578–596. doi:10.2307/3515096

Guo, L., and Riding, R. (1992). Aragonite Laminae in Hot Water Travertine Crusts, Rapolano Terme, Italy. *Sedimentology* 39, 1067–1079. doi:10.1111/j.1365-3091.1992.tb01997.x

Handford, C. R., Kendall, A. C., Prezbindowski, D. R., Dunham, J. B., and Logan, B. W. (1984). Salina-margin Tepees, Pisoliths, and Aragonite Cements, Lake MacLeod, Western Australia: Their Significance in Interpreting Ancient Analogs. *Geol.* 12, 523–527. doi:10.1130/0091-7613(1984)12<523:STPAAC>2.0.CO;2

Himmler, T., Bach, W., Bohrmann, G., and Peckmann, J. (2010). Rare Earth Elements in Authigenic Methane-Seep Carbonates as Tracers for Fluid Composition during Early Diagenesis. *Chem. Geology* 277, 126–136. doi:10.1016/j.chemgeo.2010.07.015

Holcomb, M., Cohen, A. L., Gabitov, R. I., and Hutter, J. L. (2009). Compositional and Morphological Features of Aragonite Precipitated Experimentally from Seawater and Biogenically by Corals. *Geochimica et Cosmochimica Acta* 73, 4166–4179. doi:10.1016/j.gca.2009.04.015

Jaramillo-Vogel, D., Foubert, A., Braga, J. C., Schaegis, J. C., Atnafu, B., Grobety, B., et al. (2019). Pleistocene Sea-floor Fibrous Crusts and Spherulites in the Danakil Depression (Afar, Ethiopia). *Sedimentology* 66, 480–512. doi:10.1111/sed.12484

Jones, B., and Peng, X. (2012). Amorphous Calcium Carbonate Associated with Biofilms in Hot spring Deposits. *Sediment. Geology* 269-270, 58–68. doi:10.1016/j.sedgeo.2012.05.019

Jones, B., and Peng, X. (2014). Signatures of Biologically Influenced CaCo3and Mg-Fe Silicate Precipitation in hot springs: Case Study from the Ruidian Geothermal Area, Western Yunnan Province, China. *Sedimentology* 61, 56–89. doi:10.1111/sed.12043

Jones, B. (2017b). Review of Aragonite and Calcite crystal Morphogenesis in thermal spring Systems. *Sediment. Geology* 354, 9–23. doi:10.1016/j.sedgeo.2017.03.012

Jones, B. (2017a). Review of Calcium Carbonate Polymorph Precipitation in spring Systems. *Sediment. Geology* 353, 64–75. doi:10.1016/j.sedgeo.2017.03.006

Keim, L., and Schlager, W. (2001). Quantitative Compositional Analysis of a Triassic Carbonate Platform (Southern Alps, Italy). *Sediment. Geology* 139, 261–283. doi:10.1016/S0037-0738(00)00163-9

Kendall, C. G. S. C., Sadd, J. L., and Alsharhan, A. (1994). Holocene marine Cement Coatings on beach-rocks of the Abu Dhabi Coastline (UAE); Analogs for Cement Fabrics in Ancient Limestones. *Carbonates Evaporites* 9, 119–131. doi:10.1007/BF03175225

Kirkland, B. L., Leo Lynch, F., Rahnis, M. A., Folk, R. L., Molineux, I. J., and McLean, R. J. C. (1999). Alternative Origins for Nannobacteria-like Objects in Calcite. *Geol.* 27, 347–350. doi:10.1130/0091-7613(1999)027<0347:AOFNLO>2.3.CO;2

Kjeldsen, K. U., Loy, A., Jakobsen, T. F., Thomsen, T. R., Wagner, M., and Ingvorsen, K. (2007). Diversity of Sulfate-Reducing Bacteria from an Extreme Hypersaline Sediment, Great Salt Lake (Utah). *FEMS Microbiol. Ecol.* 60, 287–298. doi:10.1111/j.1574-6941.2007.00288.x

Kowalewska, A., and Cohen, A. S. (1998). Reconstruction of Paleoenvironments of the Great Salt Lake Basin during the Late Cenozoic. *J. Paleolimnol.* 20, 381–407. doi:10.1023/A:1008053505320

Krumbein, W. E., Patterson, D. M., and Zavarzin, G. A. (2003). *Fossil and Recent Biofilms: A Natural History of the Impact of Life on Planet Earth*. Dordrecht: Kluwer Scientific Publishers, 482.

Lavoie, D. (1995). Carbonate Botryoids in Lower Devonian Amygdaloidal Basalts: Evidence for Precipitation of High-Magnesium Calcite from Heated and Volcanic CO_2-buffered marine Waters. *J. Sediment. Res.* 65, 541–546. doi:10.1306/D4268121-2B26-11D7-8648000102C1865D

Lindsay, M. R., Anderson, C., Fox, N., Scofield, G., Allen, J., Anderson, E., et al. (2017). Microbialite Response to an Anthropogenic Salinity Gradient in Great Salt Lake, Utah. *Geobiology* 15, 131–145. doi:10.1111/gbi.12201

Lindsay, M. R., Dunham, E. C., and Boyd, E. S. (2020). "Microbialites of Great Salt Lake," in *Great Salt Lake Biology*. Editors B.K. Baxter and J.K. Butler (Cham: Springer), 87–118. doi:10.1007/978-3-030-40352-2_4

Livingstone, D. A. (1963). "Chemical Composition of Rivers and Lakes," in *Date Of Geochemistry*. Editor M. Fleischer. Sixth Edition (Washington: Geological Survey Professional Paper)), 1–64.

Lokier, S. W., and Fiorini, F. (2016). Temporal Evolution of a Carbonate Coastal System, Abu Dhabi, United Arab Emirates. *Mar. Geology* 381, 102–113. doi:10.1016/j.margeo.2016.09.001

Longman, M. K. (1980). Carbonate Diagenetic Textures from Nearshore Diagenetic Environments. *AAPG* 64, 461–487. doi:10.1306/2F918A63-16CE-11D7-8645000102C1865D

Loucks, R. G., and Folk, R. L. (1976). Fanlike Rays of Former Aragonite in Permian Capitan Reef Pisolite. *J. Sediment. Res.* 46, 483–485. doi:10.1306/212F6FC8-2B24-11D7-8648000102C1865D

Malinverno, A., and Ryan, W. B. F. (1986). Extension in the Tyrrhenian Sea and Shortening in the Apennines as Result of Arc Migration Driven by Sinking of the Lithosphere. *Tectonics* 5, 227–245. doi:10.1029/TC005i002p00227

Marangon, A., Gattolin, G., Della Porta, G., and Preto, N. (2011). The Latemar: A Flat-Topped, Steep Fronted Platform Dominated by Microbialites and Synsedimentary Cements. *Sediment. Geology* 240, 97–114. doi:10.1016/j.sedgeo.2011.09.001

Mazzullo, S. J. (1980). Calcite Pseudospar Replacive of marine Acicular Aragonite, and Implications for Aragonite Cement Diagenesis. *J. Sediment. Res.* 50, 402–422. doi:10.1306/212F7A18-2B24-11D7-8648000102C1865D

Mercedes-Martín, R., Brasier, A. T., Rogerson, M., Reijmer, J. J. G., Vonhof, H., and Pedley, M. (2017). A Depositional Model for Spherulitic Carbonates Associated with Alkaline, Volcanic Lakes. *Mar. Pet. Geology* 86, 168–191. doi:10.1016/j.marpetgeo.2017.05.032

Minissale, A. (2004). Origin, Transport and Discharge of CO2 in central Italy. *Earth-Science Rev.* 66, 89–141. doi:10.1016/j.earscirev.2003.09.001

Munnecke, A., Westphal, H., Reijmer, J. J. G., and Samtleben, C. (1997). Microspar Development during Early marine Burial Diagenesis: a Comparison of Pliocene Carbonates from the Bahamas with Silurian Limestones from Gotland (Sweden). *Sedimentology* 44, 977–990. doi:10.1111/j.1365-3091.1997.tb02173.x

Nielsen, P., Muchez, P., Heijlen, W., Tony Fallick, A. E., Keppens, E., Weis, D., et al. (2005). Columnar Calcites as Testimony of Diagenetic Overprinting at the Boundary between Upper Tournaisian Dolomites and Limestones (Belgium): Multiple Origins for Apparently Similar Features. *Sedimentology* 52, 945–967. doi:10.1111/j.1365-3091.2005.00727.x

Ostwald, W. (1897). Studien über die Bildung und Umwandlung fester Körper. *Z. Phys. Chem.* 22, 289–330.

Pace, A., Bourillot, R., Bouton, A., Vennin, E., Galaup, S., Bundeleva, I., et al. (2016). Microbial and Diagenetic Steps Leading to the Mineralisation of Great Salt Lake Microbialites. *Sci. Rep.* 6, 31495. doi:10.1038/srep31495

Patacca, E., Sartori, R., and Scandone, P. (1992). Tyrrhenian basin and Apenninic Arcs: Kinematic Relations since Late Tortonian Times. *Memorie Societa' Geologica Italiana* 45, 425–451.

Paul, A., and Lokier, S. W. (2017). Holocene marine Hardground Formation in the Arabian Gulf: Shoreline Stabilisation, Sea Level and Early Diagenesis in the Coastal Sabkha of Abu Dhabi. *Sediment. Geology* 352, 1–13. doi:10.1016/j.sedgeo.2017.02.005

Paul, A., Lokier, S. W., Sherry, A., Andrade, L. L., Court, W. M., Land, C., et al. (2020). Erosion-initiated Stromatolite and Thrombolite Formation in a Present-day Coastal Sabkha Setting. *Sedimentology* 68, 382–401. doi:10.1111/sed.12783

Peckmann, J., Thiel, V., Michaelis, W., Clari, P., Gaillard, C., Martire, L., et al. (1999). Cold Seep Deposits of Beauvoisin (Oxfordian; southeastern France) and Marmorito (Miocene; Northern Italy): Microbially Induced Authigenic Carbonates. *Int. J. Earth Sci.* 88, 60–75. doi:10.1007/s005310050246

Pederson, C. L., McNeill, D. F., Klaus, J. S., and Swart, P. K. (2015). Deposition and Diagenesis of marine Oncoids: Implications for Development of Carbonate Porosity. *J. Sediment. Res.* 85, 1323–1333. doi:10.2110/jsr.2015.77

Pedley, H. M. (1990). Classification and Environmental Models of Cool Freshwater Tufas. *Sediment. Geology* 68, 143–154. doi:10.1016/0037-0738(90)90124-c

Pedley, M. (2014). The Morphology and Function of Thrombolitic Calcite Precipitating Biofilms: A Universal Model Derived from Freshwater Mesocosm Experiments. *Sedimentology* 61, 22–40. doi:10.1111/sed.12042

Pedone, V. A., and Folk, R. L. (1996). Formation of Aragonite Cement by Nannobacteria in the Great Salt Lake, Utah. *Geol.* 24, 763–765. doi:10.1130/0091-7613(1996)024<0763:foacbn>2.3.co;2

Pentecost, A. (2003). Cyanobacteria Associated with Hot spring Travertines. *Can. J. Earth Sci.* 40, 1447–1457. doi:10.1139/e03-075

Pentecost, A. (1995). Geochemistry of Carbon Dioxide in Six Travertine-Depositing Waters of Italy. *J. Hydrol.* 167, 263–278. doi:10.1016/0022-1694(94)02596-4

Pentecost, A. (2005). *Travertine*. Berlin Heidelberg: Springer, 445.

Pope, M. C., and Grotzinger, J. P. (2000). "Controls on Fabric Development and Morphology of Tufas and Stromatolites, Uppermost Pethei Group (1.8 Ga), Great Slave Lake, Northwest Canada," in *Carbonate Sedimentation and Diagenesis in the Evolving Precambrian World*. Editors J. P. Grotzinger and N. P. James (Tulsa: SEPM Spec. Publ.), 67, 103–121. doi:10.2110/pec.00.67.0103

Pruss, S. B., Bottjer, D. J., Corsetti, F. A., and Baud, A. (2006). A Global marine Sedimentary Response to the End-Permian Mass Extinction: Examples from Southern Turkey and the Western United States. *Earth-Science Rev.* 78, 193–206. doi:10.1016/j.earscirev.2006.05.002

Reid, R. P., and MacIntyre, I. G. (1998). Carbonate Recrystallization in Shallow marine Environments: a Widespread Diagenetic Process Forming Micritized Grains. *J. Sediment. Res.* 68, 928–946. doi:10.2110/jsr.68.928

Reid, R. P., MacIntyre, I. G., and Post, J. E. (1992). Micritized Skeletal Grains in Northern Belize Lagoon: a Major Source of Mg-Calcite Mud. *J. Sediment. Res.* 62, 145–156. doi:10.1306/D42678B1-2B26-11D7-8648000102C1865D,

Reitner, J., Arp, G., Thiel, V., Gautret, P., Galling, U., and Michaelis, W. (1997). Organic Matter in Great Salt Lake Ooids (Utah, USA) – First Approach to a Formation of Organic Matrices. *Facies* 36, 210–219.

Riding, R. (2008). Abiogenic, Microbial and Hybrid Authigenic Carbonate Crusts: Components of Precambrian Stromatolites. *Geol. Croat.* 61, 73–103.

Riding, R. (2000). Microbial Carbonates: the Geological Record of Calcified Bacterial-Algal Mats and Biofilms. *Sedimentology* 47, 179–214. doi:10.1046/j.1365-3091.2000.00003.x

Russo, F., Neri, C., Mastandrea, A., and Baracca, A. (1997). The Mud mound Nature of the Cassian Platform Margins of the Dolomites A Case History: the Cipit Boulders from Punta Grohmann (Sasso Piatto Massif, Northern Italy). *Facies* 36, 25–36. doi:10.1007/bf02536875

Sandberg, P. A. (1983). An Oscillating Trend in Phanerozoic Non-skeletal Carbonate Mineralogy. *Nature* 305, 19–22. doi:10.1038/305019a0

Sandberg, P. A. (1975). New Interpretations of Great Salt Lake Ooids and of Ancient Non-skeletal Carbonate Mineralogy. *Sedimentology* 22, 497–537. doi:10.1111/j.1365-3091.1975.tb00244.x

Sandberg, P. (1985). "Aragonite Cements and Their Occurrence in Ancient Limestones," in *Carbonate Cements*. Editors N. Schneidermann and P. M. Harris (Tulsa: Society of Economic Paleontologist and Mineralogists Special Publication), 36, 33–57. doi:10.2110/pec.85.36.0033

Scherf, A.-K., and Rullkötter, J. (2009). Biogeochemistry of High Salinity Microbial Mats - Part 1: Lipid Composition of Microbial Mats across Intertidal Flats of Abu Dhabi, United Arab Emirates. *Org. Geochem.* 40, 1018–1028. doi:10.1016/j.orggeochem.2009.04.002

Shinn, E. A. (1969). Submarine Lithification of Holocene Carbonate Sediments in the Persian Gulf. *Sedimentology* 12, 109–144. doi:10.1111/j.1365-3091.1969.tb00166.x

Shtukenberg, A. G., Punin, Y. O., Gunn, E., and Kahr, B. (2012). Spherulites. *Chem. Rev.* 112, 1805–1838. doi:10.1021/cr200297f

Stolarski, J., and Mazur, M. (2005). Nanostructures of Biogenic versus Abiogenic Calcium Carbonate Crystals. *Acta Palaeontol. Pol.* 50, 847–865.

Sumner, D. Y., and Grotzinger, J. P. (2004). Implications for Neoarchaean Ocean Chemistry from Primary Carbonate Mineralogy of the Campbellrand-Malmani Platform, South Africa. *Sedimentology* 51, 1273–1299. doi:10.1111/j.1365-3091.2004.00670.x

Sumner, D. Y., and Grotzinger, J. P. (2000). Late Archean Aragonite Precipitation: Petrography, Facies Associations, and Environmental Significance. *SEPM Spec. Publ.* 67, 124–144.

Swart, P. K. (2015). The Geochemistry of Carbonate Diagenesis: The Past, Present and Future. *Sedimentology* 62, 1233–1304. doi:10.1111/sed.12205

Taviani, M., and Rabbi, E. (1984). Marine Botryoidal Aragonite in Pleistocene Reef Limestones of Red Sea Offshore Islands (Northern Brother and Rocky Island). *Mineral. Petrogr. Acta* 28, 49–58.

van der Kooij, B., Immenhauser, A., Steuber, T., Bahamonde Rionda, J. R., and Meríno Tomé, O. (2010). Controlling Factors of Volumetrically Important

marine Carbonate Cementation in Deep Slope Settings. *Sedimentology* 57, 1491–1525. doi:10.1111/j.1365-3091.2010.01153.x

Vanden Berg, M. D. (2019). Domes, Rings, Ridges, and Polygons: Characteristics of Microbialites from Utah's Great Salt Lake. *Sed Rec.* 17, 4–10. doi:10.2110/sedred.2019.1.4

Vennin, E., Bouton, A., Bourillot, R., Pace, A., Roche, A., Brayard, A., et al. (2019). The Lacustrine Microbial Carbonate Factory of the Successive Lake Bonneville and Great Salt Lake, Utah, USA. *Sedimentology* 66, 165–204. doi:10.1111/sed.12499

Verrecchia, E. P., Freytet, P., Verrecchia, K. E., and Dumont, J. L. (1995). Spherulites in Calcrete Laminar Crusts: Biogenetic $CaCO_3$ Precipitation as a Major Contribution to Crust Formation. *J. Sediment. Res.* A65, 690–700. doi:10.1306/D426819E-2B26-11D7-8648000102C1865D

Warren, J. K. (1982). The Hydrological Significance of Holocene Tepees, Stromatolites, and Boxwork Limestones in Coastal Salinas in South Australia. *J. Sediment. Res.* 52, 1171–1201. doi:10.1306/212F80F8-2B24-11D7-8648000102C1865D

Wen, L. (2015). Impacts of a Saline Lake and Its Salinity on Local Precipitation. *Adv. Meteorology* 2015, 1–11. doi:10.1155/2015/679634

Wilson, P. A., and Dickson, A. D. (1996). Radiaxial Calcite: Alteration Product of and Petrographic Proxy for Magnesian Calcite marine Cement. *Geol.* 24, 945–948. doi:10.1130/0091-7613(1996)024<0945:rcapoa>2.3.co;2

Wood, R. (1999). *Paleoecology of the Capitan Reef.* Tulsa: SEPM Special publication.

Conflict of Interest: The authors declare that the research was conducted in the absence of any commercial or financial relationships that could be construed as a potential conflict of interest.